HHS Public Access

Author manuscript

Phys Med Biol. Author manuscript; available in PMC 2021 January 06.

Published in final edited form as:

Phys Med Biol. ; 64(7): 07TR01. doi:10.1088/1361-6560/ab03f1.

Microvascular Imaging of the Skin

Anthony J Deegan[1], **Ruikang K Wang**[1,2]

[1]University of Washington, Department of Bioengineering, 3720 15th Ave. NE., Seattle, WA 98195

[2]University of Washington, Department of Ophthalmology, 325 9th Ave., Seattle, WA 98104

Abstract

Despite our understanding that the microvasculature plays a multifaceted role in the development and progression of various conditions, we know little about the extent of this involvement. A need exists for non-invasive, clinically meaningful imaging modalities capable of elucidating microvascular information to aid in our understanding of disease, and to aid in the diagnosis/monitoring of disease for more patient-specific care. In this review article, a number of imaging techniques are summarized that have been utilized to investigate the microvasculature of skin, along with their advantages, disadvantages and future perspectives in preclinical and clinical settings. These techniques include dermoscopy, capillaroscopy, Doppler sonography, laser Doppler flowmetry and perfusion imaging, laser speckle contrast imaging, optical coherence tomography (OCT), including its Doppler and dynamic variant and the more recently developed OCT angiography, photoacoustic imaging, and spatial frequency domain imaging. Attention is largely, but not exclusively, placed on optical imaging modalities that use intrinsic optical signals to contrast the microvasculature. We conclude that whilst each imaging modality has been successful in filling a particular niche, there is no one, all-encompassing modality without inherent flaws. Therefore, the future of cutaneous microvascular imaging may lie in utilizing a multi-modal approach that will counter the disadvantages of individual systems to synergistically augment our imaging capabilities.

Keywords

vascular imaging; microvasculature; perfusion; skin; dermoscopy; capillaroscopy; Doppler; laser speckle; OCT; photoacoustic imaging; spatial frequency domain imaging

1. Introduction

Despite the microvascular system representing a significant portion of the circulatory network[1,2], its role in diseases, such as cardiovascular disease, remains largely unknown[3,4]. This may, in part, be due to the invasive nature of conventional microvascular imaging techniques, which are typically performed in highly specialized settings; thus, limiting their use for expanding our understanding of microvascular disease[5]. With that, a number of alternative techniques and technologies have been sought to counter such limitations. One of the earliest non-invasive methods utilized the transparency of the retina, making it a unique site where the *in vivo* microvasculature could be directly monitored over time. Through such, retinal photographic imaging techniques have allowed for the development of computer-aided methods for quantifying subtle abnormalities in the retinal

microvasculature[6,7], subsequently drawing links between retinal microvascular features and cerebrovascular, cardiovascular, and metabolic outcomes[8]. Whilst such imaging continues to be successful in identifying specific traits associated with numerous systemic pathologies[9], it is largely, but not exclusively, limited to imaging resting state or unstimulated vasculature. The wealth of knowledge gained from retinal imaging and recent advancements in technology have allowed for the development of imaging techniques and modalities that utilize alternative sites for investigating the microvasculature, e.g. the skin[10]. It is now possible to examine cutaneous microvascular function and dysfunction via skin imaging, allowing for the *in vivo* imaging of cutaneous microvasculature to be considered not only an aid in the diagnosis and treatment of dermatologic conditions[11], such as various skin lesions[12], psoriasis[13], and burn wound depth assessment[14,15], but also conditions representative of other organ systems[16], such as diabetes[17], Raynaud's phenomenon[18], and fibromyalgia[19].

With that, this review offers an insight into the numerous components that make up the skin's microvasculature, with a focus of describing the techniques developed to image and measure such components. We detail both universal and skin-specific apparatuses and physiological workings to highlight the importance of identifying and measuring such, prior to describing a number of key imaging modalities and their fundamental principles that are regularly employed for both preclinical and clinical applications. These include dermoscopy and videocapillaroscopy, which use spectral reflectivity to image the most superficial microvessels of the skin for morphological-based analyses; Doppler sonography, which combines the acoustic reflectivity of ultrasonography with the Doppler effect to provide vascular functionality and morphological analyses; laser Doppler flowmetry (LDF), which measures the Doppler shift in light to provide real-time, continuous flow assessment of a single point or vessel; laser Doppler perfusion imaging (LDPI), which forgoes continuous flow analyses to provide flow information over a larger scan area; laser speckle contrast imaging (LSCI), which combines near-continuous flow assessment with a larger field of view by flood illumination and snapshot imaging; optical coherence tomography (OCT), which uses the interference of coherent light combined with functional extensions, such as Doppler OCT (DOCT), dynamic OCT (dOCT), and OCT angiography (OCTA), to offer structural and vascular morphological analyses as well as functional flow analyses at capillary level resolution; and photoacoustic imaging, which uses optical irradiation to generate acoustic waves via thermoelastic expansion for vascular morphological and blood flow oxygenation analyses. The fundamental principles of each modality are discussed alongside advantages, disadvantages, and future prospects.

2. The Skin and Composing Microvasculature

Microvascular circulation has previously been defined as the circulation of blood within arterioles less than 300 μm in diameter, adjoining capillaries and subsequent venules[20], the anatomy of which in the skin first being studied by Spalteholz in the late 19th century[21]. *In vivo*, healthy skin consists three primary layers: the most superficial being the avascular epidermis, typically 0.06 – 0.6 mm in thickness, the intermediate being the dermis, typically 1 – 4 mm in thickness, which comprises connective tissue, blood and lymphatic vessels, hair follicles, nerves, glands, etc., and the deepest being the hypodermis or subcutaneous tissue,

typically 5 – 20 mm in thickness and comprising mainly adipose tissue[22] (figure 1 (a)). Of interest here is the vasculature of the dermis, which consists two primary plexuses: the superficial papillary plexus, which is located in the papillary dermis and serves the above epidermis, and a more substantial reticular plexus located above the junction between the dermis and hypodermis to serve the hair follicles and sweat glands[23] (figure 1 (b)). This review will primarily focus on the microvasculature of the superficial papillary plexus, which contains capillaries stemming from a series of arterioles, forming distinct capillary loops, before emptying into subjoining venules[24] (figure 1 (c)).

Whilst precise vascular dimensions depend on a number of factors, such as skin thickness, body location, and age[11,25], certain anatomical facts are universal. The inner lining of all microcirculatory blood vessels consists a monolayer of endothelial cells that regulates the exchange of products between the vessels and surrounding tissues. Surrounding the larger vessels of the microcirculatory system, i.e. arterioles and venules, is a layer of smooth muscle cells that control vessel contraction (vasoconstriction) and relaxation (vasodilation) to regulate blood flow and pressure. Arterioles are typically 10 – 100 μm in diameter, innervated, and supply blood to the capillaries, which are typically 8 – 10 μm in diameter, not innervated, and form the superficial vascular bed. The capillaries do not contain the same layer of smooth muscle cells as their larger counterparts, i.e. arterioles and venules. From the capillaries, blood flows to the venules, which are typically 10 – 200 μm in diameter, with a thinner smooth muscle cell wall compared to the arterioles[25].

Anatomically speaking, the microvasculature of the skin, and in particular the superficial capillary network, is sparse when compared to that of other tissues. Muscle, for example, was described as having 1,000 – 2,000 capillaries per squared mm[26], whereas skin was described as having just 16 – 65 capillaries per squared mm[27]. In addition, functionally speaking, the microvasculature of the skin has similar responsibilities as those of other tissues; it is responsible for the delivery of oxygen and nutrients and subsequent waste product removal, fluid homeostasis, and the accommodation of inflammatory response, but unique to the skin, is the facilitation of temperature control[25]. The importance of this unique trait will become apparent later in the review. The location of the skin's microvasculature means it is also more susceptible to outside influences, such as ultraviolet radiation and/or trauma, and is more susceptible to metabolic fluctuations due to it being responsible for temperature control[24].

Imaging the microvasculature of skin is a challenging prospect with site-, depth-, and individual-specific variances, even in healthy skin. Microvascular morphology, for example, is heterogeneous due to anatomical differences, such as epidermal thickness, and outside influences, such as long term UV irradiation[28], and when one considers the pathophysiology of certain diseases will also affect vascular morphology[29,30], specificity becomes ever more difficult and crucial. With that, additional parameters, such as microvascular density, are also measured. Decreased microvascular density, for example, has been linked with cardiovascular and metabolic diseases, such as hypertension, diabetes, obesity and metabolic syndrome[31–33], alongside an increased risk of coronary artery disease[34]. To further augment the diagnostic capacity of cutaneous microvascular imaging, however, one can also utilize

the one trait unique to the skin's microvasculature: the ability to react to a stressor such as heat.

This is an interesting trait because as mentioned, capillaries do not contain the same smooth muscle cell lining that arterioles and venules enjoy, and so cannot dilate or constrict in the same way. With that, an additional feature is utilized if adjustments to cutaneous microcirculatory blood flow are required, and this comes in the form of a reserve vasculature that under normal resting conditions remains unperfused[35], only being recruited under conditions of stress[36]. This reserve vasculature comprises arteriovenous anastomosis, or glomus, that connect the smaller arterioles and venules of the skin. Each vessel is richly innervated by sympathetic fibers, has a lumen diameter of approximately 20 μm and walls 2 – 3 x thicker than those seen in arterioles with a similar caliber[37]. In many cases, assessing microvascular reactivity through these reserve vessels, in addition to resting state parameters, is considered essential for carrying out investigations into the pathophysiology of certain diseases, such as cardiovascular disease[38,39], and diabetes[40], alongside atherosclerosis risk factors, such as low-density lipoprotein (LDL) levels[41]. Because of this, cutaneous microvasculature now being considered a representative vascular bed for the assessment of systemic microvascular reactivity[16,42], reaffirming the importance of developing non-invasive imaging technologies capable of assessing such.

3. Cutaneous Microvascular Imaging Modalities

Depending upon the scanning environment/purposes, i.e. dermatology clinic, hospital, research center, etc., the level of detail required, the location(s) of region(s) of interest, penetration requirements, and the intended analyses to be carried out, there are a number of imaging modalities available. Figure 2 very briefly outlines some commonly used modalities employed for cutaneous imaging, highlighting resolution and penetration depth. Shown is the high resolution but limited penetrative capacity of confocal microscopy, the more balanced optical coherence tomography (OCT), and the superior penetrative capacity but limited resolution of ultrasonography. This review continues with discussing a number of imaging techniques that are largely non-invasive and have the means to capture microvessel-level detail. Microvascular imaging, however, as is the case for many forms of medical imaging, is a continually developing field and this review does not cover an exhaustive list of techniques available, commercial, prototype or otherwise.

3.1 Dermoscopy

Perhaps the most economical technique available for the evaluation of cutaneous microvasculature beyond naked eye assessment is with the use of dermoscopy. First introduced to improve melanoma detection[43], dermoscopy simply utilizes a type of handheld magnifier, a dermoscope, to assess the pigmented structures of the epidermis via spectral reflectivity, typically at 10X magnification. The most modern devices use cross-polarized light instead of an immersion interface to reduce the level of superficially reflected light from the skin surface and maximize visualization of deeper structures[44]. This allows one to image the most superficial vessels of the papillary dermis to aid in the evaluation of nonpigmented lesions[45] (figure 3 (a) and (b)[46]). In an effort to supplement the objectivity of

this largely qualitative assessment tool, a three-step scoring system was proposed[47]. This process primarily focusses on the morphology and architectural arrangements of the most superficial vascular structures alongside additional dermoscopic clues, which ultimately allows for a classification of melanocytic versus nonmelanocytic and benign versus malignant nonpigmented skin tumors[48]. Zaluadek *et al.*, for example, used dermoscopy to study both pigmented and nonpigmented Bowen's disease or squamous cell carcinoma and concluded that dermoscopy could augment the diagnostic accuracy of such a disease because of the presence of repetitive vascular and structural morphological findings[49]. Similar findings were published for superficial basal cell carcinoma, concluding that dermoscopy may be particularly useful in diagnosing early basal cell carcinoma lesions where key clinical features are typically lacking[50]. Additionally, dermoscopy has also been applied to inflammatory skin conditions, such as facial nonpigmented actinic keratosis[51], augmenting the clinical usefulness of this modality.

Whilst dermoscopy is advantageous in that it is a non-invasive, inexpensive *in vivo* imaging technique[53,54] with a diagnostic odds ratio > 15 times higher than that of naked eye examinations[55], specificity is a noted limitation[49–51]. It has been reported that additional assessments are needed to confirm if those features noted using this technique are specific to each condition studied. Continued monitoring over time via sequential digital dermoscopy imaging may add to the credibility of this technique given that it has been shown to detect otherwise dermoscopically featureless melanoma[56,57]. Such instruments are inherently more expensive, however, when compared to conventional dermoscopes[58], so their use is less frequent. The benefit of dermoscopy lies in its simplicity and whilst it is a valuable tool for time and cost efficient clinical evaluations that will enhance a clinician's assessment capabilities, its usefulness is limited to providing a magnified view of only the most superficial layers of the skin, meaning it may not have the penetrative capacity or resolution to be considered for preclinical research or the assessment of more systemic conditions.

3.2 Capillaroscopy

With its origin dating back to when Kolhaus first used a primitive microscope to observe the small blood vessels surrounding the nails[59] and with an inherent principle similar to that of dermoscopy, capillaroscopy too uses an optical magnifying system to image the vasculature of the skin via spectral reflectivity, only typically it does so periungually, i.e. around the fingernails. In the nailfold, large portions of the capillaries are visible because they characteristically lie in a horizontal plane forming what can be described as hairpins orientated towards the extremity of the finger. A recent advancement to capillaroscopy saw the development of videocapillaroscopy, which works on the same principle but utilizing a handheld probe consisting of a charge-coupled device (CCD) camera connected to a monitor via fiber optics[60]. Imaging of the digital microvasculature in such a way is common when identifying the early stages of connective tissue diseases[61] through the largely qualitative assessment of morphology, shape and distribution homogeneity of the capillaries[62,63], which also includes numerous quantitative parameters, such the distance between each capillary and their neighbors and each capillary's area of influence, often considered an oxygen diffusion area[60].

In addition to connective tissue diseases, however, capillaroscopy has also been used to investigate the microvasculature of diabetes[64] and for the detection of microvascular dysfunction associated with obesity[65]. Interestingly and further compounding the importance of assessing microvascular reactivity alongside resting parameters, Francischetti *et al.*, reported no change in microvascular density measurements between obese and normal subjects at rest; however, a significant difference was noted post-stimulation with normal subjects experiencing a 3 – 4 times higher response compared to their obese counterparts during post-occlusive reactive hyperaemia (PORH) and venous occlusion, respectively[40].

The benefit of such a modality is that repeatability and reliability can often be high, but this unfortunately comes with associated conditions. For example, when nailfold videocapillaroscopy itself was assessed for repeatability, it was found to be high but only for a single observer[66], and when assessed for intra- and inter-observer reliability, it was again found to be high, but only when the images were evaluable, which was only 46.2% and 73% of the time for disease severity and vessel density measurements, respectively[67]. These data ultimately lend certain limitations when using such a modality for long term or multi-institutional studies.

Additionally, an interesting question arises when one considers the advantages/disadvantages of such a system over its principally-similar counterpart, dermoscopy. Videocapillaroscopy is comparatively specialized and not available to all rheumatologists, whilst dermoscopy is small, inexpensive and easily portable[68]. Furthermore, after comparing both techniques, Dogan *et al.* concluded that although videocapillaroscopy facilitates a more detailed vascular evaluation (most likely due to a higher standard magnification, 200X compared with 10X, allowing for a more accurate evaluation of capillaries[68]), dermoscopy is as capable for identifying pathognomonic changes in nailfold vasculature[69]. Figure 3 (c) – (f) shows comparative images taken using both techniques[52]. Therefore, the reason neither technique has surpassed the other in terms of popularity is likely due to their primary operators; capillaroscopy is largely utilized by rheumatologists, whilst dermoscopy is largely utilized by dermatologists. Ultimately, however, both techniques do suffer from one universal flaw. When imaging microvascular structures at the level of detail afforded by such modalities, we do not know if a detected capillary is physiologically active or not[60]. Such an observation highlights the need for quantitative blood flow analyses alongside morphological/architectural imaging. As mentioned, the simplicity of dermoscopy is advantageous in terms of efficacy of use, and capillaroscopy is no different. Similarly, such an advantage also limits the use of such techniques outside of aiding diagnoses and/or monitoring progression/treatment within a clinic.

3.3 Ultra- and Doppler Sonography

Initially developed for the detection of industrial flaws in ships before later being adapted and applied to the field of obstetrics in the mid-1950s[70], ultrasound imaging, or ultrasonography, has been shown to hold superior diagnostic value over visual examinations alone in the field of dermatology[71,72]. The principles of diagnostic ultrasonography are based off those of sonar[73], relying on the acoustic reflectivity of sound waves with higher than audible frequencies[74]. Essentially, when an electrical signal is passed through a

piezoelectric crystal, said crystal produces mechanical vibrations. These vibrations are transmitted into the body as pulses of sound waves via a transducer (housing unit for the piezoelectric crystal), which then echo back from tissue interfaces. The transducer receives the echo and the piezoelectric crystal returns it to an electrical signal[75]. A phenomenon known as acoustic impedance, which relies on a tissue's density and subsequent reflective properties, provides distinguishable contrast between tissue structures[76]. Ultrasonographic information is gathered using sequential frames over time, with each frame consisting of either continuous or repeated pulses that form scan lines[77]. High frequency ultrasonography (HFUS) typically utilizes variable frequency transducers to focus on various tissue depths to enable real-time imaging of structural features, such as musculotendinous, cartilaginous, or bony structures[78], with the frequency used being dependent upon the penetration depth and resolution required. A typical transabdominal probe, for example, requires a frequency range of 2 – 5 MHz, but prototype dermatologic probes use much higher frequencies, up to 100 MHz. This increased frequency allows for significantly higher resolution images but at the cost of depth penetration[79]. Commercially-available dermatologic systems typically range 5 – 20 MHz and are limited to imaging structural features only. One concept that we did not touch upon previously is temporal resolution. For ultrasonography, when anatomical structures are displayed as sequential frames over time, temporal resolution is the time from the beginning of one frame to the next. This represents the ability to distinguish between events of moving structures, e.g. events of the cardiac cycle. A high frame rate typically translates to a high temporal resolution, meaning more rapidly moving structures or events can be resolved[77]. More relevant here, however, is an addition to ultrasonography that allows for the visualization of blood flow.

A functional extension to ultrasonography utilizes the Doppler effect to produce a technique termed Doppler sonography, which can provide additional spatiotemporal vasculature and perfusion pattern information[80]. In principle, the Doppler effect, or shift, known since the mid-19th century[81], refers to the change in frequency that occurs when there is relative movement between the source of a wave and the detector. This occurs when the waves are either compressed as the source and the detector are being drawn together, or spread out as the source and the detector are being drawn apart (figure 4 (a)). Simply, this effect can be heard with the change in pitch, determined by the frequency of sound waves, similar to when an emergency vehicle is being driven towards you or away from you with its siren sounding[82]. Measuring this effect in conjunction with ultrasonographic imaging produces Doppler sonography, which has been deemed a useful tool in distinguishing benign from malignant lesions through changes in vascular density and morphology[83,84], whilst also correlating vascular density with metastatic potential[85]. Figure 4 (b) demonstrates simply how the Doppler effect is utilized to measure blood flow. Although a well-established and successful technique, ultrasonography was largely confined to a clinical setting; the development of Doppler sonography, however, brought the technique of ultrasonography from the clinic to the preclinical research forum, significantly augmenting its value. What Doppler sonography affords a research scientist or clinician goes beyond being able to qualitatively and/or semi-quantitatively assess vascular morphology and/or spatial distribution, as previously mentioned with other more basic techniques; rather, it allows for one to measure quantitative parameters of blood flow, such as direction and velocity. A

technique termed color Doppler can be employed in a similar way to how ultrasonography images anatomic structures. That is, each frame of color Doppler comprises repeated (not continuous) pulses of ultrasound to form a scan line called ensemble length. These repeated pulses per scan line allow for autocorrelation to be carried out, which provides information regarding direction and velocity of flow[77].

However, there is a fundamental limitation for Doppler sonography in terms of temporal resolution. When ultrasound pulses are transmitted at a given frequency, i.e. pulse repetition frequency, the maximum Doppler frequency that can be measured is half that of the pulse repetition frequency. If flow velocity and angle yield a frequency beyond this limit, the temporal resolution of the Doppler signal will be affected causing inaccuracies in flow measurements to occur. This phenomenon is referred to as the Nyquist limit and the ambiguous inaccuracies are referred to as aliasing[86]. A simple example of this phenomenon can be seen when the spokes of a wheel appear to be spinning in the opposite direction to actual rotation when filmed at a low frame rate[87]. One could counter such effects to image higher velocity flow; however, higher velocity flow requires higher pulse repetition frequencies, which inherently comes with a loss of depth resolution[77].

Despite the limited temporal resolution seen with Doppler sonography, this technique has successfully proven its worth in numerous studies[88–90]; however, there remains an additional drawback. Typically, Doppler sonography is derived from both blood flow and tissue motion, with this tissue motion, commonly referred to as clutter, sometimes overlapping slow flow signals. This means that when a single-dimensional wall filter, i.e. a non-adaptive or fixed thresholding mechanism, is applied to remove said clutter, it also removes slow flow signals. To overcome this limitation, a dynamic filtering method, termed Superb Microvascular Imaging (SMI), was developed. SMI significantly increases microvessel sensitivity by increasing resolution and decreasing motion-derived artifacts[91] through a self-adaptive algorithm that differentiates and separates the slow flow signals from the clutter; thus, removing only the clutter and maintaining the slow flow signals[91,92]. This results in an image that maintains both high and low velocity flow[93]. Numerous studies have shown SMI to have a higher sensitivity for microvascular imaging when compared with conventional Doppler imaging techniques[93–95]; however, there are associated pitfalls. To obtain optimal image quality, for example, a considerable learning curve is required alongside further work being needed to ascertain the optimal cut-off value for the vascular index and qualitative criteria[91]. Therein lies significant drawbacks to this technique that also highlight a common challenge with all imaging technologies: the requirement for continued development and refinement. The resolution and penetrative capacity of conventional Doppler sonography means it is possibly more suited to imaging the larger, deeper vessels of the skin or underlying soft tissue; thus, limiting its use in investigating capillary level vasculatures, which may be more important when studying cutaneous or systemic inflammatory conditions. Novel advances, however, such as power Doppler sonography, claim an increased sensitivity to smaller vessels and low-velocity flow, meaning the application of Doppler sonography in both preclinical studies and clinical practices may become more varied in the future.

3.4 Laser Doppler Flowmetry and Perfusion Imaging

Exploiting the Doppler effect for advanced microvascular imaging is also possible with an alternative wave source. With the invention of the laser in the 1960s and the subsequent utilization of the Doppler effect alongside such for various applications, chief among which were gas velocimetry measurements carried out by the National Aeronautics and Space Administration (NASA)[96], the development and use of laser Doppler for blood flow measuring began in the early 1970s[82]. This technique is commonly referred to as Laser Doppler Flowmetry (LDF).

Similar to acoustic waves, when a photon is scattered by a moving particle, its frequency is Doppler-shifted. By analyzing this Doppler shift, or the array of Doppler shifts generated from numerous photons, it is possible to study the dynamics of these moving particles[97]. Blood flow information is gathered using this method because the frequency of the light that is reflected or randomly scattered by the static tissue will not be Doppler-shifted, and so will not change. In contrast, the frequency of the light that is scattered by moving blood cells within the patient's vessels will be Doppler-shifted, the degree of which being proportional to the speed of the red blood cells[98].

Measuring the Doppler effect in light, however, requires a different approach to that of its acoustic counterpart because light waves travel at significantly higher frequency than sound waves. This higher frequency makes any shift within such difficult to measure directly; therefore, a phenomenon referred to as 'beats' is used to measure the Doppler effect in light. Beats is the outcome produced when two similar frequencies of light are superimposed, resulting in them adding to (constructive) and canceling one another out (destructive) as they come in and out of phase, respectively. These amplitude changes produce a detectable frequency that is equal to the difference in frequency between both waves, referred to as beats or beat frequency. Taking this phenomenon into account, when a Doppler-shifted wave of light is superimposed with a reference wave corresponding to the frequency of the original emitted light, a beat frequency is produced that is lower than both of the constituent frequencies. This beat frequency is comparatively easier to measure, and by analyzing changes in this frequency, one can determine the velocity of the object reflecting or scattering the light[82]. In this case, that is blood flow.

A key feature of LDF is that it takes flow measurements from a single point or vessel at any one time, meaning it can provide continuous, real-time flow information[52]. Because of this, LDF has been used predominantly to monitor reactive flow under various conditions or stimuli[99,100]. This key feature, however, is also the source of a significant disadvantage to using LDF; in that, using a single point or vessel for flow analysis could result in a high variability between measurements[42,101,102] because microvasculature is inherently inhomogeneous and flow can vary both spatially and temporally[10]. Additionally, because LDF measures flow at a single point, it does not provide any visual vascular information allowing for morphological or density measurements. If one requires both qualitative morphological assessments and quantitative flow measures, an additional technique may be required alongside LDF. This apparently simultaneous advantage and disadvantage to using LDF means that its use may be limited to that of a corroborative role in preclinical studies, more so than as a clinically useful diagnostic tool. To overcome this limitation would require

performing LDF in a scanning mode over a larger area; thus, removing its key advantageous feature: continuous, real-time flow assessment.

Nevertheless, advances in the field of laser Doppler-based imaging have led to the development of just such a scanning mode, i.e. Laser Doppler Perfusion Imaging (LDPI). Unlike conventional LDF, which assesses a single point, LDPI assesses flow from multiple points over a broader area using a scanning mode to build up a perfusion map[52] to a depth of approximately 1 – 1.5 mm[103]. Figure 5 (a) shows the typical setup of an LDPI system. This technique is advantageous in that it reduces inter- and/or intra-measurement variabilities caused by vascular inhomogeneities[101] by measuring multiple points successively over a scan area; however, this advantage naturally means that LDPI can no longer measure flow continuously. LDPI, therefore, has a lower temporal resolution compared to LDF and can no longer be considered a real-time imaging modality. Using this technique, LDPI has been used in numerous studies, such as the monitoring of resting state flow undergoing treatment[104], and the vascular infusion of an artificial dermal graft[103]. Figure 5 (b) shows the LDPI of a fingertip before and after immersion in iced-water[105]. This highlights the increased field of view of this technique but also the non-continuous imaging element. Whilst this technique can provide a perfusion map of a given area, the resolution is such that vascular morphology is not distinguishable. This means again, if measures are required of multiple parameters, such as qualitative morphological assessment and quantitative flow assessment, an alternative modality, if not multiple modalities, may be required. Such traits broaden the scope of use for this technique to include more preclinical uses, as well as clinical, where larger perfusion maps are the preferred assessment criteria over single point, continuous flow assessments. These could include the assessment of large cutaneous disorders, both acute and chronic, as well as systemic disorders where cutaneous reactive perfusion may be an assessment criterion.

3.5 Laser Speckle Contrast Imaging

An imaging technique with the potential to combine the continuous, real-time imaging ability of LDF with the perfusion mapping ability of LDPI is Laser Speckle Contrast Imaging (LSCI). LSCI illuminates an area of tissue with coherent light, typically 20 × 20 cm[106], via flood illumination, whilst simultaneously taking a snapshot image of the reflected light from said area with a digital camera without the time consuming need for scanning[52]. This produces a readable perfusion map because as coherent light interacts with a random scattering medium, photons are scattered by particles of varying positions within said medium, meaning they travel a distribution of distances before they reach the photodetector. This results in constructive and destructive interference that is dependent upon the spatial and temporal positions of the scattering particles in relation to the photodetector. When these scattered photons are captured with a camera, a random intensity or amplitude pattern, referred to as speckle, is seen. If the scattering particles are moving, such as red blood cells do, this will cause fluctuations in the interference, which appear as intensity fluctuations at the photodetector[97]. When several frames of the speckle pattern are acquired with an exposure time of up to 50 ms[107], blurring occurs as a result of the intensity fluctuations, which can then be quantified using spatial variations[108], temporal variations[109], or both[110]. A typical LSCI system setup is shown in figure 6 (a), with comparative results from a

conventional LSCI system and more advanced dual-wavelength LSCI system being shown in figure 6 (b) and (c), respectively[111]. Figure 6 (d) shows the typical perfusion index signals derived from regions of interest in figure 6 (c).

The theoretical basis behind LSCI originated in the late 1960s with the development of dynamic light scattering[112,113], and with continued development relating speckle temporal dynamics to particle dynamics in the 1970s[114], LSCI was first introduced to blood flow imaging in the 1980s where it was used to image blood flow in the retina[108]. Further development saw the use of LSCI to progress from retinal imaging to skin imaging in the 1990s[97]. Since then, LSCI has been used for a multitude of preclinical- and clinical-based studies; for example, as a microvascular function research tool in patients with coronary artery disease[115] and a plausible mechanism for predicting healing times of pediatric scald wounds[106]. Given the simplicity of LSCI and its supposed advantages over other imaging techniques, it has been compared with both LDF[116] and LDPI[117] for skin imaging capacities. Tew *et al.*, for example, compared LSCI with LDF for the assessment of microvascular function via post-occlusive reactive hyperaemia (PORH) in healthy adults and concluded that whilst LSCI was over all more reproducible than LDF, most likely due to lower inter-site variability, the increased sensitivity of LSCI made reproducibility problematic in areas of low blood flow[116]. Additionally, Millet *et al.* compared LSCI with LDPI for skin flux measurements and concluded that both methods were similarly capable[117]. With that, LSCI provides a method for one to monitor near-continuous flow via perfusion mapping, but again, it lacks the resolution required for rigorous microvessel morphological analyses. Similar to LDPI, LSCI is, therefore, largely restricted to imaging cutaneous conditions through a wide field-of-view with limited resolution. This supports the need for, and use of, alternative modalities for circumstances requiring a more in-depth analysis via a narrow field-of view and higher resolution.

3.6 Optical Coherence Tomography

Optical coherence tomography (OCT) is a non-invasive imaging technique that utilizes the interference of coherent light to rapidly produce cross-sectional images and three-dimensional (3D) volume information[118,119]. The principles of OCT are often compared to those of ultrasonography, only using light rather than sound to gather information. Typically, low coherent, near infrared light is directed onto the target tissue, skin in this case, with the backscattering of such being used to generate information based on the optical properties of the various structures within the skin. Simply, the light beam is split and simultaneously directed onto both the skin and an internal reference mirror. When the backscattered light from both sources is combined, a phenomenon termed interference occurs. A photodetector receives the signal and measures the interference. The position of the reference mirror and magnitude of the backscattered light collected at that point in time give the relative location and density of the microstructure within the skin scattering said light. Each point measured, therefore, provides a depth profile snapshot of the skin, termed an A-line, or A-scan (longitudinal axis). A cross-sectional image, termed a B-scan, or B-frame, is generated when multiple A-lines are taken at consecutive, overlapping points along a linear trajectory over the surface of the skin. These cross-sectional images can be viewed in real-time, providing depth-resolved structural information about the skin[120]. Because modern OCT technology

can produce micron scale images with a lateral resolution of 1 – 10 μm to a depth of 2 – 3 mm[121], biological and pathological microarchitectural features of numerous tissues can be qualitatively imaged and quantitatively measured both *ex vivo* post-fixation and *in vivo* in real-time[118] to a level that is comparable to histologic assessment[122]. It does not, however, provide microvascular information without functional extensions, such as Doppler OCT, which offer considerably more information to the clinician or researcher.

3.7 Doppler Optical Coherence Tomography (DOCT)

One of the first functional extensions of OCT to detect blood flow speed and direction utilized the Doppler effect to produce a modality called Doppler OCT (DOCT). Similar in principle to Doppler sonography but producing more detailed information, DOCT combines the Doppler principle with OCT[123] to identify flow velocities with a sensitivity as low as 10 μm/s at a spatial resolution of just 10 μm[124,125]. This is typically carried out using an algorithm that extracts Doppler information from the OCT signal by comparing phase differences between repeated, single/similar location A-lines. Started with time domain OCT technique used for retinal imaging in the mid-1990s[126], phase-resolved Fourier domain Doppler is the preferred DOCT method due to its high velocity sensitivity and imaging speed [124,127,128]. There are other options, however[129]. Using amplitude differences to gather the same data, for example, produces amplitude-resolved Doppler that is of considerable interest to some research groups; however, amplitude information is more akin to the speckle effect rather than the Doppler effect[130]. A third option exists that utilizes both phase and amplitude information to produce complex-resolved Doppler[131], but whilst both phase and amplitude information is gathered from adjacent A-lines, complex information is gathered from adjacent B-scans[132], requiring a completely different algorithm/approach[133,134]. Shown in figure 7 is an example of DOCT imaging of the palm of an individual's hand[130]. Compared are the three DOCT methods described above, i.e. phase-, amplitude-, and complex-resolved Doppler.

One of the few limitations associated with using DOCT for microvascular imaging has to do with the Doppler effect being dependent upon the angle between the probe and the direction of flow, an attribute feature referred to as Doppler angle[131]. The effects of this feature on each of the Doppler methods used for skin imaging, i.e. phase-, amplitude-, and complex-resolved Doppler, were recently discussed in a study carried out by Liu *et al.* who compared all three methods of extraction to conclude that not only was information quality from all three methods dependent upon flow direction in relation to the probing beam, but that both phase- and amplitude-resolved methods were also sensitive to Doppler angle[130]. This means data collected using this method may be susceptible to considerable operator-dependent variations. Despite this limitation, however, DOCT pioneered a new wave of interest in OCT technology, inspiring the development of numerous extensions that not only revolutionized how OCT technology is used (see below, OCT angiography), but also significantly increased the scope of its uses for both preclinical and clinical practices.

3.8 Dynamic Optical Coherence Tomography (dOCT)

Dynamic-OCT (dOCT) is a specifically designed, commercially-available OCT system that utilizes speckle variance derived from amplitude information[135] to detect cutaneous blood

flow *in vivo*. Speckle-variance-OCT (SV-OCT) has the capability of depth-resolved 3D imaging, typically requiring just seconds to acquire[136,137]. As mentioned, the speckle pattern is dependent upon the spatial and temporal fluctuations in the intensity of light being backscattered from the tissue being imaged[138]. Contrasting the vasculature within such relies on the statistical analysis of the inter-frame speckle variance being generated by moving red blood cells[139]. dOCT does just that by utilizing rapidly repeating OCT scans to detect regions that have changed between successive scans. Whilst the majority of the scan data will remain unchanged, blood flow produces small changes; thereby, revealing the locations of blood vessels[12]. dOCT has been successfully used for numerous healthy[28], pathological[29,140], and stimulated skin studies[141]. Shown in figure 8 (a) – (f) are the *en face* images of vascular patterns from different regions of healthy skin, with figure 8 (g) showing a cross-sectional B-scan image overlaid with vascular information highlighted in red; all acquired using dOCT[11].

A considerable advantage to using such a technique lies with its insensitivity to Doppler angle-dependent contrast[142], and whilst the structural and vascular information afforded by OCT imaging has been reported as far exceeding that of dermoscopy and videocapillaroscopy[140], a number of key limitations remain with dOCT. These include a penetration depth of just 500 μm, and a resolution that may be insufficient to detect blood flow in capillaries with a diameter of 10 μm[141]. With dOCT also being a commercialized system, the use of such for preclinical applications is limited. Typically, but not exclusively, medical imaging studies carried out with commercialized technologies are aimed towards clinical applications as opposed to preclinical because they lack the enhanced abilities and freedoms afforded by prototype technologies to customize the specificities of each study. For that reason, more recent technical and technological developments are needed to expand the uses of such a modality to include both preclinical and clinical applications.

3.9 Optical Coherence Tomography Angiography (OCTA)

The use of optical coherence tomography angiography (OCTA) for cutaneous imaging is the most exciting example of the aforementioned developments that exists as a functional extension of OCT increasingly being used for *in vivo* preclinical and clinical applications[143,144]. Originally developed for retinal microvascular imaging[145], OCTA has made numerous advances to include a number of commercially-available forms; however, its application into cutaneous microvascular imaging is significantly more recent. As mentioned with other modalities, OCTA too uses the movement of red blood cells as a contrasting mechanism; thus, foregoing the need for exogenous contrasting agents[146] and eliminating the risk of dye injection-associated side effects[147]. Like dOCT before, OCTA extrapolates vascular information from successive, single location, cross-sectional B-scans; but unlike dOCT, OCTA benefits from significant improvements in performance made possible through recent technological advances in available light sources, interferometer design and electronics, alongside the development of novel OCTA algorithms[148]. Modern OCT systems that utilize 200-kHz swept-source lasers (SS-OCT), for example, are frequently used for OCTA analyses of the skin[149] allowing for a lateral resolution of 10 μm, a penetration depth of 1.5 mm with an axial resolution of 8 μm, and a comparatively high temporal resolution when compared to their 20-kHz commercially-available dOCT counterparts[12]. The methods

through which OCTA extrapolates vascular information from an OCT signal, however, is what sets it apart, and with extensive experience in clinical ophthalmology, OCTA's translation into clinical dermatology is expected in the near future.

Similar to DOCT, the vascular information gained from OCTA can be extrapolated in a number of ways. Typically, OCTA will utilize either a phase-, amplitude-, or complex-based algorithm, all of which employ the same data processing procedures, only on different information within the OCT signal. A recent study carried out by Xu *et al.* compared the performances of all three OCTA algorithms and concluded that complex-based information provides the best performance for OCTA imaging[148]. This may be because, as Xu *et al.* explains, complex-based methods of extraction utilize both phase and amplitude changes in the returning light signal to extract pertinent information. This is important because whilst phase changes are more sensitive to movement, i.e. the flow of red blood cells, providing more detailed information about flow, phase information is also more susceptible to other motion noise, which subsequently makes detecting slow or low blood flow difficult. By also utilizing amplitude information, however, a phase noise compensation mechanism is applied to improve low flow signals and enhance the detection of capillary-level flow. When both signal changes are analyzed simultaneously, information concerning both larger vessels with fast flow and smaller vessels with slow flow is gathered. Foreseeing this outcome more than a decade ago, Wang *et al.* proposed a novel method, termed optical angiography (OAG), to convert the modulated OCT signal into a complex function using a modified Hilbert transform with the aim of separating the blood flow signal from that of static tissue[133]. A more recent version, termed optical microangiography (OMAG), is in use today, which typically uses either differential[132,150] or Eigen-decomposition[151] (the more common method for cutaneous microvascular imaging) over the modified Hilbert transform to extract vascular information.

To date, OCTA has been instrumental in expanding the awareness of and use of OCT in the field of dermatology through a number of preclinical and clinical studies. The initial path undertaken to hone this technique for dermatologic use employed a spectrometer-based system to monitor wound healing in the pinna of healthy nude mice[152] before being used on phantoms and the skin of healthy volunteers[132], alongside the preliminary assessment of inflammatory conditions[153]. Technological advancements soon gave rise to OCTA being utilized with a swept-source laser[154] and improved techniques saw the introduction of a correlation mapping algorithm for better noise reduction[155] and novel registration methods for reduced bulk motion-derived artifacts[156]. Preliminary studies using stimulation mapping[157], facial acne lesion monitoring[158] and early wound healing assessments[159] ultimately led to a highly refined modality that recently imaged the microvasculatures of a number of normal and inflammatory skin conditions[149] alongside the identification of structural and microvascular adaptations known to occur during wound healing[160,161] in unrivaled detail. Novel quantification methods have also correlated the microvascular response to local stimuli with capillary blood volume extraction[162] to demonstrate how OCTA may be used for commercial or industrial research and development.

Shown in figure 9 are the results of two wound healing studies[152,160] that, with the numerous innovations just mentioned, demonstrate the advances in technique and smooth

transition of OCTA from preclinical, animal model studies to the clinically relevant imaging of human skin. With the commercialization of dOCT systems, approval from the Food and Drug Administration (FDA), and the wide spread use and success of OCTA for ophthalmologic purposes, it is reasonable to think OCTA will soon be a common diagnostic/imaging tool in dermatologic and other clinics.

Figures 10 and 11 show the diverse range of qualitative assessments that can be carried out using OMAG-based OCTA. In figure 10, a 24-hour old scald wound is shown. Vascular parameters, such as vessel density, can be seen to differ significantly between scan sites, despite their close proximity. Figure 11 shows the same scald wound segmented into slabs that independently show the vessels of depths thought to represent the papillary dermis, the upper reticular dermis, and the reticular dermis. This ability allows for more specific assessments to be carried out taking into account both lateral and axial parameters. Numerous parameters can be quantified also to the same level of specificity, such as vessel density, diameter, and flux, among many others[160]. The level of detail afforded by OMAG-based OCTA could not only be used to as an important clinical diagnostic tool for the identification and monitoring of countless cutaneous disorders, as well as systemic disorders with vascular manifestations, but it could also provide access to preclinical microvascular information previously unavailable by non-invasive means. A limitation to this technique may exist in its degree of refinement, however. For example, whilst the narrow field-of-view affords capillary-level resolution, it may also make for identifying potential scan sites difficult in studies exploiting large areas of skin with no visible areas of interest. In said cases, OCTA may initially be too highly refined; rather, a more appropriate option might be to combine OCTA with a larger field-of-view modality that could firstly identify key areas of interest before OCTA makes for a more in-depth analysis. As with all previously mentioned modalities, there is no one, all-encompassing microvascular imaging technique and each of those discussed is more suited to a particular use than another.

3.10 Photoacoustic Imaging

An example of a non-invasive, 3D imaging strategy that utilizes a physical principle first discovered by Alexander Graham Bell more than a century ago[163] is photoacoustic imaging. Photoacoustic imaging has been described as a hybrid imaging modality that employs the photoacoustic effect to exploit the absorption contrast capacity of optical imaging with the depth resolution of ultrasonography[164]. The photoacoustic effect refers to a physical principle where optical energy is converted into acoustic energy through optical absorption and thermal expansion (figure 12 (a)). Simply, when a biological tissue is bombarded with nanosecond pulsed light, a local rapid rise in temperature of several millikelvin degrees occurs. This in turn causes thermal expansion and the subsequent generation of wideband ultrasound pulses that can be detected on the tissue surface by an ultrasound transducer[165]. In this way, photoacoustic imaging can distinguish the specific absorption signatures of endogenous chromophores, such as hemoglobin and melanin; thus, highlighting the location of blood vessels *in vivo*[166]. The spatiotemporal resolution of such a technique can vary widely depending upon the specific variation being reported. Typically, however, spatial resolution varies between 20 – 100 μm and temporal resolution is < 100 μs[167].

Early applications of this principle varied from the development of the photophone in the early 1880s[168] to gas analysis in the late 1930s[169]. Its first application to a field relative to this review, i.e. the generation of acoustic waves by the absorption of light pulses in tissue, was in the early 1960s[170]. Continued efforts saw the first *in vivo* application of the photoacoustic effect in the early 1990s[171]. Such a technique might be advantageous for medical or biomedical applications for a number of reasons: chiefly, its sensitivity to detecting optical absorption via intensity variations in reflected light is at times two orders of magnitude higher than other pure optical imaging modalities[164], and whilst pure ultrasonography too enjoys the fact that acoustic waves do not suffer from the same degree of scatter in biological tissue as photons, thus maintaining their original propagation directions over a greater distance enabling a higher spatial resolution at depth, the photoacoustic contrast mechanism, if performed spectroscopically, is capable of measuring additional physiological parameters, such as oxygen saturation and metabolic rate[172]. Photoacoustic imaging, therefore, combines the advantageous attributes of both optical and acoustic imaging into one modality to become a more comprehensive imaging tool. A thorough review carried out by Hu and Wang discusses in detail the three primary embodiments of photoacoustic imaging, i.e. microscopy, computed tomography, and endoscopy, alongside a number of measureable parameters, and potential advances and future applications[166].

Interestingly, a number of attempts have also been made to further augment the usability of this technology by combining it with OCT for joint cutaneous vascular and structural studies[174,175]. Whilst these studies are inspiring, a number of limitations were discussed. Namely, the diagnostic benefit and utility of such a modality is called into question along with the sheer size and usability of the physical prototype system and the unattractive acquisition time of > 4 minutes. With regards to diagnostic benefit, it has been reasoned that the spectroscopic capacity of photoacoustic imaging combined with the functional flow analysis capabilities of OCT extensions, such as DOCT, could provide a route for additional information gathering that is currently unavailable[174]. Furthermore, whilst the current state of this modality constrains its use to preclinical applications, it should be noted that photoacoustic imaging is a relatively young imaging modality, and with a fundamental principle that affords a unique approach to information acquisition, the scope for further development and use in both preclinical and clinical applications is broad. Figure 12 (b) gives an impressive example of the current state of photoacoustic imaging[173].

3.11 Spatial Frequency Domain Imaging (SFDI)

Another relatively young imaging modality that utilizes an alternative approach to assess the skin blood perfusion is the spatial frequency domain imaging (SFDI). SFDI is a wide-field, non-invasive imaging modality that utilizes the optical properties and biochemical composition of the skin to produce spatial tissue maps of both structural features and chromophore (e.g. hemoglobin) concentrations, respectively[176,177]. Initially proposed and applied by Cuccia *et al.* to turbid media before being extensively applied to studies of the skin[178], it typically measures the diffuse reflectance of spatially modulated light to quantify both the reduced scattering coefficient and optical absorption (μ'_s and μ_a) of tissue, i.e. skin in this case[179]. In doing so, this technique is capable of simultaneously imaging the

superficial structural features of the skin as well as indirectly monitoring the vascular health of the skin by assessing perfusion through oxygenated hemoglobin content.

Simply, the illumination light is structured into sinusoidal patterns, i.e. stripes of light, and projected on to the skin surface. The use of differing spatial frequencies allows for the modulation transfer function of the skin to be found, upon which μ'_s and μ_a is determined[178,180]. Standard SFDI acquires three frames of data at relative phases of 0, 120, ad 240 degrees for each spatial frequency, from which to gather information on a pixel-by-pixel basis[181,182]. The requirement of 3-phase shifted frames limits the imaging speed for in vivo applications due to inevitable subject movement. Alternative demodulation techniques are being developed. Nadeau et al., for example, have used a two-dimensional (2D) Hilbert transform method that required just two frames of data in total to acquire the necessary information for obtaining optical properties[181]. Faster still was a method developed that required just a single frame of data to acquire the necessary information; a technique was referred to as single snapshot of optical properties (SSOP)[198].

Compared with other modalities, SFDI has the unique ability to quantitatively decouple light scattering from absorption, which provides structural and physical information (light scattering), such as structural details, firmness, and elastic modulus, and biochemical composition information (light absorption), such as moisture and soluble solid composition[183]. Important here is how SFDI indirectly assesses vascular health by measuring the oxygenated and deoxygenated hemoglobin contents, i.e. oxyhemoglobin (HbO_2) and deoxyhemoglobin (Hb), respectively, which gives an ability to provide measures of tissue oxygen saturation (stO_2)[176]. This ability has been used to measure numerous parameters in both preclinical[184–186] and clinical[187] models, including the skin[177,188–190]. Figure 13 (a) – (c) demonstrates SFDI imaging of an individual's right hand [197]. Whilst being hailed as a true real-time SFDI technique, it is also more sensitive to changes in ambient light in practice, which may pose challenges when used in a clinical environment where light conditions change frequently[182]. Another direction for possible SFDI development was demonstrated by Burmeister *et al.* in a study that combined SFDI with LSCI for burn severity measurement[199]. As mentioned with other techniques, the combination of multiple modalities is becoming increasingly popular for both preclinical and clinical studies; hence, an already versatile modality, such as SFDI, would likely become increasingly useful.

4. Conclusions and Future Perspectives

Cutaneous microvasculature has been shown in many published works to hold vast amounts of information concerning both cutaneous and systemic diseases. Tapping into that information via non-invasive imaging could provide a wealth of information ultimately increasing our understanding of the multi-tiered roles played by the microvasculature in countless conditions. With that, a number of different imaging modalities have been discussed here; all utilizing varying scientific principles with varying advantages and disadvantages making each more suitable than another for specific purposes. Universal across all modalities, however, is the unyielding requirement for refinement of techniques and technologies that simultaneously aim to address the more immediate clinical needs of

patients whilst also enhancing our more fundamental understanding of cutaneous microvasculature.

One key area for potential growth may reside with the combination of multiple imaging strategies into a single platform to utilize their combined advantages and counter their individual disadvantages. Using LSCI, for example, to assess large plains of skin for the identification of potential areas of interest prior to a more in-depth investigation with a higher resolution technique, such as OCTA, may be a practical approach for improved assessment efficiency that also aids in eliminating the inherent subjectivity in assessment site allocation. Similarly, combining an imaging modality with a treatment strategy may be another area warranting development. The capacity to non-invasively image the microvasculature of the face whilst simultaneously providing cosmetic light therapy, for example, could augment the effectiveness of such treatment and aid in progression monitoring. In both examples, one system will ultimately guide the other. Additionally, by merging these potential developments with the current drive to produce endoscopic and/or handheld probes for increased portability and use of what were once cumbersome technologies, the potential applicability of these technologies increases significantly both preclinically and clinically. It is also worth noting that whilst the path to clinical translation for any imaging technology is rightfully not without trials and tribulations, non-invasive modalities are classified as lower risk by the FDA compared to their invasive counterparts, and therefore, experience fewer regulatory controls when attempting to obtain approval prior to clinical use. Questions concerning validation, safety, cost, design and form, usability and practicality, and more must be addressed before any device can be applied to clinical use; however, the same scrutiny and more must be applied to more invasive technologies.

With that, however, whilst this review has focused on non-invasive imaging modalities, the use of minimally invasive contrast agents and the wealth of information they offer should not be overlooked. In the field of ultrasonography, for example, the use of an advanced filtering mechanism known as superb microvascular imaging (SMI) is often used alongside a contrast agent to produce a technique called contrast-enhanced ultrasonography (CEUS), which has been reported as amplifying flow signals and available microvascular information[200] for an improved diagnostic accuracy[201]. Another interesting area of development sees the use of fluorophore probes as a potential contrast mechanism for microvascular imaging. Currently, a number of non-specific fluorophore probes are already approved by the FDA for use in humans, and whilst they were initially used to predominantly contrast superficial skin structures[202,203], they were also used to contrast skin perfusion[204] and vasculature[205]. More recently, the use of non-specific fluorophore probes has progressed to include fluorescein angiography (FA), a now commonplace technique in ophthalmic assessments that contrasts retinal microvasculature for subsequent high resolution imaging[206–208]. Whilst cutaneous microvascular imaging through the use of fluorophore probes has not yet enjoyed the same degree of success as retinal microvascular imaging, possibly due to the skin’s absorption and scattering capacity for the wavelength of light used to excite the fluorophores, continual innovations in administration technique[209], degree of probe specificity[210], and modes of use[211], mean that whilst many work to develop non-invasive imaging modalities that utilize endogenous contrast agents, the degree of cutaneous microvascular information gained from fluorophore probes and other exogenous contrast agents is likely to rise. Additionally, an

alternative approach to tackling those same absorption and scattering issues associated all cutaneous imaging modalities may be to reduce the scattering potential of the skin itself[212,213]. This could be achieved through the use of tissue optical clearing methods[214] meaning a combination of both tactics may be a plausible way forward for improved utility and applicability.

Furthermore, an aspect of microvascular imaging not yet tackled in this review concerns those conditions not accessible via the microvasculature of the skin, i.e. those conditions that require microvascular imaging of alternative tissue organs. Although the modalities discussed here are capable of assessing a wide range of cutaneous and systemic conditions, as well as acute and chronic cutaneous injuries, via cutaneous microvascular imaging, not all conditions, particularly acute local injury to tissues other than the skin, are visible in this way. An example of such would be ischemic tissue within the brain or heart following stroke or infarction, respectively. Whilst particular microvascular or circulatory characteristics known to be precursors to this type of tissue injury have previously been investigated in the skin, the degree of vascular and tissue damage at the site of ischemia itself requires direct assessment. Therefore, cutaneous microvascular imaging following an ischemic stroke or cardiac infarction would not offer any additional information as to the degree of acute local tissue damage, response, or repair.

On a final note, future developments in the field of cutaneous microvascular imaging, and indeed all fields of medical imaging, may not be directly related to a specific modality; rather, indirectly related via the volume of data collected, how it is interpreted, and how it is communicated. Improved computing power, for example, could see significantly larger volumes of data being collected with shorter acquisition times with previously wasted information being extrapolated and utilized in new ways to provide novel insights in real-time or at point-of-care. The use of automated processes and artificial intelligence could also be used during data assessment to reduce the unavoidable element of subjectivity present during manual interpretation, and once collected and interpreted, how the data is relayed via communication systems to the necessary points of care will also improve over all workflow and patient care.

Acknowledgements

This work is support in part through research grants by the National Heart, Lung, and Blood Institute (R01HL093140), the National Eye Institute (R01EY024158, and R01EY028753), and Washington Research Foundation. Generous support from the University of Washington Department of Bioengineering is also acknowledged. The funding organizations had no role in the design or conduct of this research.

References

1. Ellis CG, Jagger J & Sharpe M The microcirculation as a functional system. Crit. Care 9, S3–S8 (2005). [PubMed: 16168072]
2. Gutterman DD et al. The Human Microcirculation – Regulation of Flow and Beyond. Circ. Res. 118, 157–172 (2016). [PubMed: 26837746]
3. Lenasi H Introductory Chapter: Microcirculation in Health and Disease. Microcirc. Revisit. - Mol. Clin. Pract. (2016).
4. den Uil CA et al. The Microcirculation in Health and Critical Disease. Prog. Cardiovasc. Dis. 51, 161–170 (2008). [PubMed: 18774014]

5. Liew G, Wang JJ, Mitchell P & Wong TY Retinal vascular imaging: a new tool in microvascular disease research. Circ. Cardiovasc. Imaging 1, 156–161 (2008). [PubMed: 19808533]
6. Kipli K et al. A Review on the Extraction of Quantitative Retinal Microvascular Image Feature. Computational and Mathematical Methods in Medicine (2018).
7. Newman A, Andrew N & Casson R Review of the association between retinal microvascular characteristics and eye disease. Clin. Experiment. Ophthalmol. 46, 531–552 (2018). [PubMed: 29193621]
8. Nguyen TT & Wong TY Retinal vascular manifestations of metabolic disorders. Trends Endocrinol. Metab. TEM 17, 262–268 (2006). [PubMed: 16890449]
9. Abràmoff MD, Garvin MK & Sonka M Retinal imaging and image analysis. IEEE Rev. Biomed. Eng. 3, 169–208 (2010). [PubMed: 22275207]
10. Allen J & Howell K Microvascular imaging: techniques and opportunities for clinical physiological measurements. Physiol. Meas. 35, R91 (2014). [PubMed: 24910968]
11. Schuh S et al. Imaging Blood Vessel Morphology in Skin: Dynamic Optical Coherence Tomography as a Novel Potential Diagnostic Tool in Dermatology. Dermatol. Ther. 7, 187–202 (2017).
12. Ulrich M et al. Dynamic optical coherence tomography in dermatology. Dermatology 232, 298–311 (2016). [PubMed: 27104356]
13. Kapsokalyvas D et al. In-vivo imaging of psoriatic lesions with polarization multispectral dermoscopy and multiphoton microscopy. Biomed. Opt. Express 5, 2405–2419 (2014). [PubMed: 25071974]
14. Monstrey SM et al. Burn wound healing time assessed by laser Doppler imaging. Part 2: Validation of a dedicated colour code for image interpretation. Burns 37, 249–256 (2011). [PubMed: 21084164]
15. Pape SA et al. Burn wound healing time assessed by laser Doppler imaging (LDI). Part 1: Derivation of a dedicated colour code for image interpretation. Burns 38, 187–194 (2012). [PubMed: 22115981]
16. Holowatz LA, Thompson-Torgerson CS & Kenney WL The human cutaneous circulation as a model of generalized microvascular function. J. Appl. Physiol. Bethesda Md 1985 105, 370–372 (2008).
17. Feng W et al. Visualization of skin microvascular dysfunction of type 1 diabetic mice using *in vivo* skin optical clearing method. J. Biomed. Opt. 24, 031003 (2018).
18. Anderson ME, Moore TL, Lunt M & Herrick AL Digital iontophoresis of vasoactive substances as measured by laser Doppler imaging—a non-invasive technique by which to measure microvascular dysfunction in Raynaud's phenomenon. Rheumatology 43, 986–991 (2004). [PubMed: 15199217]
19. Al-Allaf AW, Khan F, Moreland J, Belch JJF & Pullar T Investigation of cutaneous microvascular activity and flare response in patients with fibromyalgia syndrome. Rheumatology 40, 1097–1101 (2001). [PubMed: 11600737]
20. Koscielny J, Latza R, Wolf S, Kiesewetter H & Jung F Early rheological and microcirculatory changes in children with type I diabetes mellitus. Clin. Hemorheol. Microcirc. 19, 139–150 (1998). [PubMed: 9849927]
21. Spalteholz W Die Verteilung der Blutgefäße in der Haut. Arch Anat Physiol Anat Abt 1–54 (1893).
22. Cammarota T, Pinto F, Magliaro A & Sarno A Current uses of diagnostic high-frequency US in dermatology. Eur. J. Radiol. 27 Suppl 2, S215–223 (1998). [PubMed: 9652525]
23. Braverman IM The cutaneous microcirculation. J. Investig. Dermatol. Symp. Proc. 5, 3–9 (2000).
24. Landis EM The capillaries of the skin: a review. J. Invest. Dermatol. 1, 295–311 (1938).
25. Bentov I & Reed MJ The effect of aging on the cutaneous microvasculature. Microvasc. Res. 100, 25–31 (2015). [PubMed: 25917013]
26. Krogh A The Anatomy and Physiology of Capillaries. Revised Edition. (Yale University Press, 1929).
27. Wetzel NC & Zotterman Y On differences in the vascular colouration of various regions of the normal human skin. Heart 13, 357 (1927).

28. Lindsø Andersen P et al. Vascular morphology in normal skin studied with dynamic optical coherence tomography. Exp. Dermatol. 27, 966–972 (2018). [PubMed: 29733465]
29. Themstrup L et al. In vivo microvascular imaging of cutaneous actinic keratosis, Bowen's disease and squamous cell carcinoma using dynamic optical coherence tomography. J. Eur. Acad. Dermatol. Venereol. JEADV 31, 1655–1662 (2017). [PubMed: 28502083]
30. Themstrup L et al. In vivo differentiation of common basal cell carcinoma subtypes by microvascular and structural imaging using dynamic optical coherence tomography. Exp. Dermatol. 27, 156–165 (2018). [PubMed: 29215761]
31. De Boer MP et al. Microvascular dysfunction: a potential mechanism in the pathogenesis of obesity-associated insulin resistance and hypertension. Microcirc. N. Y. N 1994 19, 5–18 (2012).
32. Debbabi H et al. Increased skin capillary density in treated essential hypertensive patients. Am. J. Hypertens. 19, 477–483 (2006). [PubMed: 16647618]
33. Kaiser SE, Sanjuliani AF, Estato V, Gomes MB & Tibiriçá E Antihypertensive treatment improves microvascular rarefaction and reactivity in low-risk hypertensive individuals. Microcirc. N. Y. N 1994 20, 703–716 (2013).
34. IJzerman RG et al. Individuals at increased coronary heart disease risk are characterized by an impaired microvascular function in skin. Eur. J. Clin. Invest. 33, 536–542 (2003). [PubMed: 12814388]
35. Chade AR Renal vascular structure and rarefaction. Compr. Physiol. 3, 817–831 (2013). [PubMed: 23720331]
36. Levy BI et al. Impaired tissue perfusion: a pathology common to hypertension, obesity, and diabetes mellitus. Circulation 118, 968–976 (2008). [PubMed: 18725503]
37. Grant RT & Bland EF Observations on arteriovenous anastomoses in human skin and in the bird's foot with special reference to the reaction to cold. Heart 15, 385–411 (1931).
38. Struijker-Boudier HAJ et al. Evaluation of the microcirculation in hypertension and cardiovascular disease. Eur. Heart J. 28, 2834–2840 (2007). [PubMed: 17942581]
39. Rizzoni D et al. How to assess microvascular structure in humans. High Blood Press. Cardiovasc. Prev. 18, 169–177 (2011). [PubMed: 22283671]
40. Francischetti EA et al. Skin capillary density and microvascular reactivity in obese subjects with and without metabolic syndrome. Microvasc. Res. 81, 325–330 (2011). [PubMed: 21236266]
41. Kenney WL, Cannon JG & Alexander LM Cutaneous microvascular dysfunction correlates with serum LDL and sLOX-1 receptor concentrations. Microvasc. Res. 85, 112–117 (2013). [PubMed: 23137925]
42. Roustit M & Cracowski J-L Assessment of endothelial and neurovascular function in human skin microcirculation. Trends Pharmacol. Sci. 34, 373–384 (2013). [PubMed: 23791036]
43. Russo T, Piccolo V, Lallas A & Argenziano G Recent advances in dermoscopy. F1000Research 5, (2016).
44. Benvenuto-Andrade C et al. Differences between polarized light dermoscopy and immersion contact dermoscopy for the evaluation of skin lesions. Arch. Dermatol. 143, 329–338 (2007). [PubMed: 17372097]
45. Arrazola P, Mullani NA & Abramovits W DermLite II: an innovative portable instrument for dermoscopy without the need of immersion fluids. Skinmed 4, 78–83 (2005). [PubMed: 15785134]
46. Errichetti E & Stinco G Dermoscopy in general dermatology: a practical overview. Dermatol. Ther. 6, 471–507 (2016).
47. Zalaudek I et al. How to diagnose nonpigmented skin tumors: a review of vascular structures seen with dermoscopy: part I. Melanocytic skin tumors. J. Am. Acad. Dermatol. 63, 361–374 (2010). [PubMed: 20708469]
48. Ayhan E, Ucmak D & Akkurt Z Vascular structures in dermoscopy. An. Bras. Dermatol. 90, 545–553 (2015). [PubMed: 26375224]
49. Zalaudek I et al. Dermoscopy of Bowen's disease. Br. J. Dermatol. 150, 1112–1116 (2004). [PubMed: 15214896]

50. Giacomel J & Zalaudek I Dermoscopy of superficial basal cell carcinoma. Dermatol. Surg. 31, 1710–1713 (2005). [PubMed: 16336893]
51. Zalaudek I et al. Dermoscopy of facial nonpigmented actinic keratosis. Br. J. Dermatol. 155, 951–956 (2006). [PubMed: 17034524]
52. Dinsdale G & Herrick AL Vascular diagnostics for Raynaud's phenomenon. J. Vasc. Diagn. 2014, 127–139 (2014).
53. Soyer HP, argenziano giuseppe, Hofmann-Wellenhof R. & Johr RH Color Atlas of Melanocytic Lesions of the Skin. (Springer Science & Business Media, 2007).
54. Argenziano G et al. Dermoscopy of pigmented skin lesions: results of a consensus meeting via the Internet. J. Am. Acad. Dermatol. 48, 679–693 (2003). [PubMed: 12734496]
55. Vestergaard ME, Macaskill P, Holt PE & Menzies SW Dermoscopy compared with naked eye examination for the diagnosis of primary melanoma: a meta-analysis of studies performed in a clinical setting. Br. J. Dermatol. 159, 669–676 (2008). [PubMed: 18616769]
56. Kittler H et al. Identification of clinically featureless incipient melanoma using sequential dermoscopy imaging. Arch. Dermatol. 142, 1113–1119 (2006). [PubMed: 16982998]
57. Altamura D, Avramidis M & Menzies SW Assessment of the optimal interval for and sensitivity of short-term sequential digital dermoscopy monitoring for the diagnosis of melanoma. Arch. Dermatol. 144, 502–506 (2008). [PubMed: 18427044]
58. Venugopal SS, Soyer HP & Menzies SW Results of a nationwide dermoscopy survey investigating the prevalence, advantages and disadvantages of dermoscopy use among Australian dermatologists. Australas. J. Dermatol. 52, 14–18 (2011). [PubMed: 21332687]
59. Cutolo M & Smith V State of the art on nailfold capillaroscopy: a reliable diagnostic tool and putative biomarker in rheumatology? Rheumatology 52, 1933–1940 (2013). [PubMed: 23620555]
60. Humbert P et al. Capillaroscopy and videocapillaroscopy assessment of skin microcirculation: dermatologic and cosmetic approaches. J. Cosmet. Dermatol. 4, 153–162 (2005). [PubMed: 17129259]
61. Herrick AL Vascular function in systemic sclerosis. Curr. Opin. Rheumatol. 12, 527–533 (2000). [PubMed: 11092203]
62. Murray AK et al. Preliminary clinical evaluation of semi-automated nailfold capillaroscopy in the assessment of patients with Raynaud's phenomenon. Microcirculation 18, 440–447 (2011). [PubMed: 21466606]
63. Etehad Tavakol M, Fatemi A, Karbalaie A, Emrani Z & Erlandsson B-E Nailfold capillaroscopy in rheumatic diseases: which parameters should be evaluated? BioMed Res. Int. 2015, 1–17 (2015).
64. Maldonado G, Guerrero R, Paredes C & Ríos C Nailfold capillaroscopy in diabetes mellitus. Microvasc. Res. 112, 41–46 (2017). [PubMed: 28274735]
65. Maranhão PA, de Souza M das GC, Kraemer-Aguiar LG & Bouskela E Dynamic nailfold videocapillaroscopy may be used for early detection of microvascular dysfunction in obesity. Microvasc. Res 106, 31–35 (2016). [PubMed: 26969104]
66. Dinsdale G et al. Quantitative outcome measures for systemic sclerosis-related microangiopathy – reliability of image acquisition in nailfold capillaroscopy. Microvasc. Res. 113, 56–59 (2017). [PubMed: 28495471]
67. Dinsdale G et al. Intra-and inter-observer reliability of nailfold videocapillaroscopy — a possible outcome measure for systemic sclerosis-related microangiopathy. Microvasc. Res. 112, 1–6 (2017). [PubMed: 28163035]
68. Hughes M et al. A study comparing videocapillaroscopy and dermoscopy in the assessment of nailfold capillaries in patients with systemic sclerosis–spectrum disorders. Rheumatology 54, 1435–1442 (2015). [PubMed: 25749623]
69. Dogan S, Akdogan A & Atakan N Nailfold capillaroscopy in systemic sclerosis: is there any difference between videocapillaroscopy and dermatoscopy? Skin Res. Technol. 19, 446–449 (2013). [PubMed: 23521585]
70. Nicolson M & Fleming JEE Imaging and imagining the fetus: the development of obstetric ultrasound. (Johns Hopkins University Press, 2013).
71. Kleinerman R, Whang TB, Bard RL & Marmur ES Ultrasound in dermatology: principles and applications. J. Am. Acad. Dermatol. 67, 478–487 (2012). [PubMed: 22285673]

72. Chami L, Lassau N, Chebil M & Robert C Imaging of melanoma: usefulness of ultrasonography before and after contrast injection for diagnosis and early evaluation of treatment. Clin. Cosmet. Investig. Dermatol. 4, 1–6 (2011).
73. Dussik KT Über die Möglichkeit, hochfrequente mechanische Schwingungen als diagnostisches Hilfsmittel zu verwerten. Z. Für Gesamte Neurol. Psychiatr. 174, 153–168 (1942).
74. Laird WR & Walmsley AD Ultrasound in dentistry. Part 1 - biophysical interactions. J. Dent. 19, 14–17 (1991). [PubMed: 2016423]
75. Evirgen Ş & Kamburoğlu K Review on the applications of ultrasonography in dentomaxillofacial region. World J. Radiol 8, 50–58 (2016). [PubMed: 26834943]
76. Abu-Zidan FM, Hefny AF & Corr P Clinical ultrasound physics. J. Emerg. Trauma Shock 4, 501–503 (2011). [PubMed: 22090745]
77. Ng A & Swanevelder J Resolution in ultrasound imaging. Contin. Educ. Anaesth. Crit. Care Pain 11, 186–192 (2011).
78. Mandava A, Konathan R & Neelala K Utility of high-resolution ultrasonography and colour Doppler in the assessment of pigmented skin lesions. Ultrasound 20, 155–160 (2012).
79. Moore CL & Copel JA Point-of-care ultrasonography. N. Engl. J. Med. 364, 749–757 (2011). [PubMed: 21345104]
80. Mandava A, Ravuri PR & Konathan R High-resolution ultrasound imaging of cutaneous lesions. Indian J. Radiol. Imaging 23, 269–277 (2013). [PubMed: 24347861]
81. Doppler C Ueber das farbige Licht der Doppelsterne und einiger anderer Gestirne des Himmels Versuch einer das Bradley'sche Aberrations-Theorem als integrirenden Theil in sich schliessenden allgemeineren Theorie. (Borrosch & André, 1842).
82. Briers JD Laser Doppler, speckle and related techniques for blood perfusion mapping and imaging. Physiol. Meas. 22, R35 (2001). [PubMed: 11761081]
83. Giovagnorio F, Andreoli C & De Cicco ML Color Doppler sonography of focal lesions of the skin and subcutaneous tissue. J. Ultrasound Med. 18, 89–93 (1999). [PubMed: 10206814]
84. Szymańska E et al. Skin imaging with high frequency ultrasound - preliminary results. Eur. J. Ultrasound 12, 9–16 (2000). [PubMed: 10996765]
85. Barnhill RL & Levy MA Regressing thin cutaneous malignant melanomas (< or = 1.0 mm) are associated with angiogenesis. Am. J. Pathol. 143, 99–104 (1993). [PubMed: 7686347]
86. Terslev L, Diamantopoulos AP, Døhn UM, Schmidt WA & Torp-Pedersen S Settings and artefacts relevant for Doppler ultrasound in large vessel vasculitis. Arthritis Res. Ther 19, (2017). [PubMed: 28148290]
87. Schäberle W Ultrasonography in Vascular Diagnosis: A Therapy-Oriented Textbook and Atlas. (Springer, 2018).
88. Giovagnorio F, Valentini C & Paonessa A High-resolution and color Doppler sonography in the evaluation of skin metastases. J. Ultrasound Med. 22, 1017–1022; quiz 1023–1025 (2003). [PubMed: 14606556]
89. Toprak H, Kiliç E, Serter A, Kocakoç E & Ozgocmen S Ultrasound and Doppler US in evaluation of superficial soft-tissue lesions. J. Clin. Imaging Sci 4, 12 (2014). [PubMed: 24744969]
90. Scotto di Santolo M et al. High-resolution color-Doppler ultrasound for the study of skin growths. Arch. Dermatol. Res. 307, 559–566 (2015). [PubMed: 25604691]
91. Park AY & Seo BK Up-to-date Doppler techniques for breast tumor vascularity: superb microvascular imaging and contrast-enhanced ultrasound. Ultrasonography 37, 98–106 (2017). [PubMed: 29025210]
92. Chen J et al. Value of superb microvascular imaging ultrasonography in the diagnosis of carpal tunnel syndrome. Medicine (Baltimore) 96, 1–7 (2017).
93. Karaca L et al. Comparison of the superb microvascular imaging technique and the color Doppler techniques for evaluating children's testicular blood flow. Eur. Rev. Med. Pharmacol. Sci. 20, 1947–1953 (2016). [PubMed: 27249591]
94. Ma Y, Li G, Li J & Ren W The diagnostic value of superb microvascular imaging (SMI) in detecting blood flow signals of breast lesions. Medicine (Baltimore) 94, 1–6 (2015).

95. Zhan J, Diao X-H, Jin J-M, Chen L & Chen Y Superb microvascular imaging - a new vascular detecting ultrasonographic technique for avascular breast masses: a preliminary study. Eur. J. Radiol. 85, 915–921 (2016). [PubMed: 27130051]

96. Huffaker RM Laser Doppler Detection Systems for Gas Velocity Measurement. Appl. Opt. 9, 1026–1039 (1970). [PubMed: 20076326]

97. Boas DA & Dunn AK Laser speckle contrast imaging in biomedical optics. J. Biomed. Opt. 15, 011109 (2010). [PubMed: 20210435]

98. Nilsson GE, Tenland T & Ake Öberg P Laser-Doppler methods for the assessment of microcirculatory blood flow. Trans. Inst. Meas. Control 4, 109–112 (1982).

99. Morales F et al. How to assess post-occlusive reactive hyperaemia by means of laser Doppler perfusion monitoring: application of a standardised protocol to patients with peripheral arterial obstructive disease. Microvasc. Res. 69, 17–23 (2005). [PubMed: 15797256]

100. Roustit M, Blaise S, Millet C & Cracowski JL Reproducibility and methodological issues of skin post-occlusive and thermal hyperemia assessed by single-point laser Doppler flowmetry. Microvasc. Res 79, 102–108 (2010). [PubMed: 20064535]

101. Roustit M, Millet C, Blaise S, Dufournet B & Cracowski JL Excellent reproducibility of laser speckle contrast imaging to assess skin microvascular reactivity. Microvasc. Res. 80, 505–511 (2010). [PubMed: 20542492]

102. Roustit M & Cracowski J-L Non-invasive assessment of skin microvascular function in humans: an insight into methods. Microcirc. N. Y. N 1994 19, 47–64 (2012).

103. Morimoto N et al. Immediate evaluation of neovascularization in a grafted bilayered artificial dermis using laser Doppler imaging. Ann. Plast. Surg. 72, 84–88 (2014). [PubMed: 23241770]

104. Murray AK, Herrick AL & King TA Laser Doppler imaging: a developing technique for application in the rheumatic diseases. Rheumatology 43, 1210–1218 (2004). [PubMed: 15226515]

105. Serov A, Steinacher B & Lasser T Full-field laser Doppler perfusion imaging and monitoring with an intelligent CMOS camera. Opt. Express 13, 3681–3689 (2005). [PubMed: 19495275]

106. Mirdell R, Farnebo S, Sjöberg F & Tesselaar E Accuracy of laser speckle contrast imaging in the assessment of pediatric scald wounds. Burns 44, 90–98 (2018). [PubMed: 28797578]

107. Satat G, Barsi C & Raskar R Skin perfusion photography. in 2014 IEEE International Conference on Computational Photography (ICCP) 1–8 (IEEE, 2014).

108. Fercher AF & Briers JD Flow visualization by means of single-exposure speckle photography. Opt. Commun. 37, 326–330 (1981).

109. Stern MD In vivo evaluation of microcirculation by coherent light scattering. Nature 254, 56–58 (1975). [PubMed: 1113878]

110. Duncan DD, Kirkpatrick SJ & Wang RK Statistics of local speckle contrast. JOSA A 25, 9–15 (2008). [PubMed: 18157206]

111. Zhang L et al. Dual-wavelength laser speckle contrast imaging (dwLSCI) improves chronic measurement of superficial blood flow in hands. Sensors 17, 2811 (2017).

112. Cummins HZ & Swinney HL III Light Beating Spectroscopy. in Progress in Optics (ed. Wolf E) 8, 133–200 (Elsevier, 1970).

113. Pecora R Quasi-Elastic Light Scattering from Macromolecules. Annu. Rev. Biophys. Bioeng. 1, 257–276 (1972). [PubMed: 4567754]

114. Berne BJ & Pecora R Dynamic light scattering. (John Wiley & Sons, Ltd, 1976).

115. Borges JP et al. A novel effective method for the assessment of microvascular function in male patients with coronary artery disease: a pilot study using laser speckle contrast imaging. Braz. J. Med. Biol. Res. 49, (2016).

116. Tew GA, Klonizakis M, Crank H, Briers JD & Hodges GJ Comparison of laser speckle contrast imaging with laser Doppler for assessing microvascular function. Microvasc. Res 82, 326–332 (2011). [PubMed: 21803051]

117. Millet C, Roustit M, Blaise S & Cracowski JL Comparison between laser speckle contrast imaging and laser Doppler imaging to assess skin blood flow in humans. Microvasc. Res. 82, 147–151 (2011). [PubMed: 21745482]

118. Huang D et al. Optical coherence tomography. Science 254, 1178–1181 (1991). [PubMed: 1957169]
119. Tomlins PH & Wang RK Theory, developments and applications of optical coherence tomography. J. Phys. Appl. Phys. 38, 2519 (2005).
120. Arevalo JF, Krivoy D & Fernandez CF How Does Optical Coherence Tomography Work? Basic Principles in Retinal Angiography and Optical Coherence Tomography 217–222 (Springer, New York, NY, 2009).
121. Jung W & Boppart SA Optical coherence tomography for rapid tissue screening and directed histological sectioning. Anal. Cell. Pathol. Amst. 35, 129–143 (2012). [PubMed: 22133731]
122. Schuh S, Kaestle R, Sattler EC & Welzel J Optical coherence tomography of actinic keratoses and basal cell carcinomas - differentiation by quantification of signal intensity and layer thickness. J. Eur. Acad. Dermatol. Venereol. JEADV 30, 1321–1326 (2016). [PubMed: 26915996]
123. Chen Z et al. Noninvasive imaging of in vivo blood flow velocity using optical Doppler tomography. Opt. Lett. 22, 1119–1121 (1997). [PubMed: 18185770]
124. Zhao Y et al. Phase-resolved optical coherence tomography and optical Doppler tomography for imaging blood flow in human skin with fast scanning speed and high velocity sensitivity. Opt. Lett. 25, 114–116 (2000). [PubMed: 18059800]
125. Wang RK High-resolution visualization of fluid dynamics with Doppler optical coherence tomography. Meas. Sci. Technol. 15, 725–733 (2004).
126. Drexler W & Fujimoto JG State-of-the-art retinal optical coherence tomography. Prog. Retin. Eye Res. 27, 45–88 (2008). [PubMed: 18036865]
127. Zhao Y et al. Three-dimensional reconstruction of in vivo blood vessels in human skin using phase-resolved optical Doppler tomography. IEEE J. Sel. Top. Quantum Electron. 7, 931–935 (2001).
128. Ma Z et al. Measurement of absolute blood flow velocity in outflow tract of HH18 chicken embryo based on 4D reconstruction using spectral domain optical coherence tomography. Biomed. Opt. Express 1, 798–811 (2010). [PubMed: 21127734]
129. Proskurin SG, He Y & Wang RK Determination of flow velocity vector based on Doppler shift and spectrum broadening with optical coherence tomography. Opt. Lett. 28, 1227–1229 (2003). [PubMed: 12885029]
130. Liu G, Lin AJ, Tromberg BJ & Chen Z A comparison of Doppler optical coherence tomography methods. Biomed. Opt. Express 3, 2669–2680 (2012). [PubMed: 23082305]
131. Zhao Y et al. Doppler standard deviation imaging for clinical monitoring of in vivo human skin blood flow. Opt. Lett. 25, 1358–1360 (2000). [PubMed: 18066216]
132. An L, Qin J & Wang RK Ultrahigh sensitive optical microangiography for in vivo imaging of microcirculations within human skin tissue beds. Opt. Express 18, 8220–8228 (2010). [PubMed: 20588668]
133. Wang RK et al. Three dimensional optical angiography. Opt. Express 15, 4083–4097 (2007). [PubMed: 19532651]
134. Wang RK & Hurst S Mapping of cerebro-vascular blood perfusion in mice with skin and skull intact by Optical Micro-AngioGraphy at 1.3μm wavelength. Opt. Express 15, 11402–11412 (2007). [PubMed: 19547498]
135. Barton JK & Stromski S Flow measurement without phase information in optical coherence tomography images. Opt. Express 13, 5234–5239 (2005). [PubMed: 19498514]
136. Mariampillai A et al. Speckle variance detection of microvasculature using swept-source optical coherence tomography. Opt. Lett. 33, 1530–1532 (2008). [PubMed: 18594688]
137. Enfield J, Jonathan E & Leahy M In vivo imaging of the microcirculation of the volar forearm using correlation mapping optical coherence tomography (cmOCT). Biomed. Opt. Express 2, 1184–1193 (2011). [PubMed: 21559130]
138. Sharma P et al. Feasibility of speckle variance OCT for imaging cutaneous microvasculature regeneration during healing of wounds in diabetic mice. Laser Phys. 28, 025601 (2018).
139. Son T et al. Optical coherence tomography angiography of stimulus evoked hemodynamic responses in individual retinal layers. Biomed. Opt. Express 7, 3151–3162 (2016). [PubMed: 27570706]

140. Aldahan AS et al. Vascular features of nail psoriasis using dynamic optical coherence tomography. Skin Appendage Disord. 2, 102–108 (2017). [PubMed: 28232916]
141. Themstrup L et al. In vivo, micro-morphological vascular changes induced by topical brimonidine studied by dynamic optical coherence tomography. J. Eur. Acad. Dermatol. Venereol. JEADV 30, 974–979 (2016). [PubMed: 26916576]
142. Cadotte DW et al. Speckle variance optical coherence tomography of the rodent spinal cord: in vivo feasibility. Biomed. Opt. Express 3, 911–919 (2012). [PubMed: 22567584]
143. Kim J, Brown W, Maher JR, Levinson H & Wax A Functional optical coherence tomography: principles and progress. Phys. Med. Biol. 60, R211 (2015). [PubMed: 25951836]
144. Zhang A et al. Wide-field optical coherence tomography based microangiography for retinal imaging. Sci. Rep 6, srep22017 (2016).
145. An L & Wang RK In vivo volumetric imaging of vascular perfusion within human retina and choroids with optical micro-angiography. Opt. Express 16, 11438–11452 (2008). [PubMed: 18648464]
146. de Carlo TE, Romano A, Waheed NK & Duker JS A review of optical coherence tomography angiography (OCTA). Int. J. Retina Vitr. 1, 5 (2015).
147. Spaide RF, Klancnik JM & Cooney MJ Retinal vascular layers imaged by fluorescein angiography and optical coherence tomography angiography. JAMA Ophthalmol. 133, 45–50 (2015). [PubMed: 25317632]
148. Xu J, Song S, Li Y & Wang RK Complex-based OCT angiography algorithm recovers microvascular information better than amplitude- or phase-based algorithms in phase-stable systems. Phys. Med. Biol. 63, 015023 (2018).
149. Deegan AJ et al. Optical coherence tomography angiography of normal skin and inflammatory dermatologic conditions. Lasers Surg. Med. 50, 183–193 (2018). [PubMed: 29356051]
150. Wang RK, An L, Francis P & Wilson DJ Depth-resolved imaging of capillary networks in retina and choroid using ultrahigh sensitive optical microangiography. Opt. Lett. 35, 1467–1469 (2010). [PubMed: 20436605]
151. Zhang Q, Wang J & Wang RK Highly efficient eigen decomposition based statistical optical microangiography. Quant. Imaging Med. Surg. 6, 557–563 (2016). [PubMed: 27942476]
152. Yousefi S, Qin J, Dziennis S & Wang RK Assessment of microcirculation dynamics during cutaneous wound healing phases in vivo using optical microangiography. J. Biomed. Opt. 19, 76015 (2014). [PubMed: 25036212]
153. Qin J, Jiang J, An L, Gareau D & Wang RK In vivo volumetric imaging of microcirculation within human skin under psoriatic conditions using optical microangiography. Lasers Surg. Med. 43, 122–129 (2011). [PubMed: 21384393]
154. Choi WJ & Wang RK Volumetric cutaneous microangiography of human skin in vivo by VCSEL swept-source optical coherence tomography. Quantum Electron. 44, 740 (2014).
155. Choi WJ, Reif R, Yousefi S & Wang RK Improved microcirculation imaging of human skin in vivo using optical microangiography with a correlation mapping mask. J. Biomed. Opt. 19, 36010 (2014). [PubMed: 24623159]
156. Wei DW, Deegan AJ & Wang RK Automatic motion correction for in vivo human skin optical coherence tomography angiography through combined rigid and nonrigid registration. J. Biomed. Opt. 22, 66013 (2017). [PubMed: 28636065]
157. Wang H, Baran U & Wang RK In vivo blood flow imaging of inflammatory human skin induced by tape stripping using optical microangiography. J. Biophotonics 8, 265–272 (2015). [PubMed: 24659511]
158. Baran U, Li Y, Choi WJ, Kalkan G & Wang RK High resolution imaging of acne lesion development and scarring in human facial skin using OCT-based microangiography. Lasers Surg. Med. 47, 231–238 (2015). [PubMed: 25740313]
159. Baran U, Choi WJ & Wang RK Potential use of OCT-based microangiography in clinical dermatology. Skin Res. Technol 22, 238–246 (2016). [PubMed: 26335451]
160. Deegan AJ et al. Optical coherence tomography angiography monitors human cutaneous wound healing over time. Quant. Imaging Med. Surg. 8, 135–150 (2018). [PubMed: 29675355]

161. Wang W, Deegan AJ, Men S & Wang RK Optical coherence tomography angiography and cutaneous wound healing in Dynamics and Fluctuations in Biomedical Photonics XV 10493, 104930D (International Society for Optics and Photonics, 2018).
162. Men S et al. OCT-based angiography of human dermal microvascular reactions to local stimuli: Implications for increasing capillary blood collection volumes. Lasers Surg. Med. (2018).
163. Wang LV & Gao L Photoacoustic microscopy and computed tomography: from bench to bedside. Annu. Rev. Biomed. Eng. 16, 155–185 (2014). [PubMed: 24905877]
164. Wang LV Tutorial on photoacoustic microscopy and computed tomography. IEEE J. Sel. Top. Quantum Electron. 14, 171–179 (2008).
165. Sun Y, Jiang H & O'Neill B Photoacoustic imaging: an emerging optical modality in diagnostic and theranostic medicine. J. Biosens. Bioelectron. 2, 1–12 (2011).
166. Hu S & Wang LV Photoacoustic imaging and characterization of the microvasculature. J. Biomed. Opt. 15, 011101 (2010). [PubMed: 20210427]
167. Wang D, Wu Y & Xia J Review on photoacoustic imaging of the brain using nanoprobes. Neurophotonics 3, (2016).
168. Bell AG On the production and reproduction of sound by light. Am. J. Sci Series 3 Vol. 20, 305–324 (1880).
169. Veingerov ML A method of gas analysis based on the Tyndall-Röntgen optico-acoustic effect. Dokl. Akad. Nauk SSSR 19, 687–688 (1938).
170. Amar L et al. Detection, on the occipital bone, of elastic (ultrasonic) waves induced by laser impulses in the eye of a rabbit. Comptes Rendus Hebd. Seances Acad. Sci 259, 3653–3655 (1964).
171. Chen QX, Davies A, Dewhurst RJ & Payne PA Photo-acoustic probe for intra-arterial imaging and therapy. Electron. Lett. 29, 1632–1633 (1993).
172. Zhou Y, Yao J & Wang LV Tutorial on photoacoustic tomography. J. Biomed. Opt. 21, 61007 (2016). [PubMed: 27086868]
173. Matsumoto Y et al. Label-free photoacoustic imaging of human palmar vessels: a structural morphological analysis. Sci. Rep. 8, 786 (2018). [PubMed: 29335512]
174. Zhang EZ et al. Multimodal photoacoustic and optical coherence tomography scanner using an all optical detection scheme for 3D morphological skin imaging. Biomed. Opt. Express 2, 2202–2215 (2011). [PubMed: 21833358]
175. Zabihian B et al. In vivo dual-modality photoacoustic and optical coherence tomography imaging of human dermatological pathologies. Biomed. Opt. Express 6, 3163–3178 (2015). [PubMed: 26417489]
176. Mazhar A et al. Spatial frequency domain imaging of port wine stain biochemical composition in response to laser therapy: a pilot study. Lasers Surg. Med. 44, 611–621 (2012). [PubMed: 22911574]
177. Yafi A et al. Postoperative quantitative assessment of reconstructive tissue status in a cutaneous flap model using spatial frequency domain imaging. Plast. Reconstr. Surg. 127, 117–130 (2011). [PubMed: 21200206]
178. Cuccia DJ, Bevilacqua F, Durkin AJ & Tromberg BJ Modulated imaging: quantitative analysis and tomography of turbid media in the spatial-frequency domain. Opt. Lett. 30, 1354–1356 (2005). [PubMed: 15981531]
179. Pera V, Karrobi K, Tabassum S, Teng F & Roblyer D Optical property uncertainty estimates for spatial frequency domain imaging. Biomed. Opt. Express 9, 661–678 (2018). [PubMed: 29552403]
180. Cuccia DJ, Bevilacqua FP, Durkin AJ, Ayers FR & Tromberg BJ Quantitation and mapping of tissue optical properties using modulated imaging. J. Biomed. Opt. 14, 024012 (2009). [PubMed: 19405742]
181. Nadeau K, Durkin AJ & Tromberg BJ Advanced demodulation technique for the extraction of tissue optical properties and structural orientation contrast in the spatial frequency domain. J. Biomed. Opt. 19, 056013 (2014). [PubMed: 24858131]
182. Applegate MB & Roblyer DM High-speed spatial frequency domain imaging with temporally modulated light. J. Biomed. Opt. 22, 076019 (2017).

183. Cen H, Lu R, Mendoza F & Beaudry RM Relationship of the optical absorption and scattering properties with mechanical and structural properties of apple tissue. Postharvest Biol. Technol 85, 30–38 (2013).

184. Tabassum S et al. Feasibility of spatial frequency domain imaging (SFDI) for optically characterizing a preclinical oncology model. Biomed. Opt. Express 7, 4154–4170 (2016). [PubMed: 27867722]

185. Singh-Moon RP, Roblyer DM, Bigio IJ & Joshi S Spatial mapping of drug delivery to brain tissue using hyperspectral spatial frequency-domain imaging. J. Biomed. Opt. 19, 96003 (2014). [PubMed: 25199058]

186. Lin AJ et al. Spatial frequency domain imaging of intrinsic optical property contrast in a mouse model of Alzheimer's disease. Ann. Biomed. Eng. 39, 1349–1357 (2011). [PubMed: 21331663]

187. Robbins CM, Raghavan G, Antaki JF & Kainerstorfer JM Feasibility of spatial frequency-domain imaging for monitoring palpable breast lesions. J. Biomed. Opt. 22, 1–9 (2017).

188. Rohrbach DJ et al. Characterization of nonmelanoma skin cancer for light therapy using spatial frequency domain imaging. Biomed. Opt. Express 6, 1761–1766 (2015). [PubMed: 26137378]

189. Saager RB, Dang AN, Huang SS, Kelly KM & Durkin AJ Portable (handheld) clinical device for quantitative spectroscopy of skin, utilizing spatial frequency domain reflectance techniques. Rev. Sci. Instrum. 88, 094302 (2017). [PubMed: 28964218]

190. Gioux S et al. First-in-human pilot study of a spatial frequency domain oxygenation imaging system. J. Biomed. Opt. 16, 086015 (2011). [PubMed: 21895327]

191. Lin AJ et al. Visible spatial frequency domain imaging with a digital light microprojector. J. Biomed. Opt. 18, (2013).

192. O'Sullivan TD, Cerussi AE, Cuccia DJ & Tromberg BJ Diffuse optical imaging using spatially and temporally modulated light. J. Biomed. Opt. 17, 071311 (2012). [PubMed: 22894472]

193. Konecky SD et al. Quantitative optical tomography of sub-surface heterogeneities using spatially modulated structured light. Opt. Express 17, 14780–14790 (2009). [PubMed: 19687956]

194. Mazhar A et al. Structured illumination enhances resolution and contrast in thick tissue fluorescence imaging. J. Biomed. Opt. 15, 010506 (2010). [PubMed: 20210421]

195. D'Andrea C, Ducros N, Bassi A, Arridge S & Valentini G Fast 3D optical reconstruction in turbid media using spatially modulated light. Biomed. Opt. Express 1, 471–481 (2010). [PubMed: 21258482]

196. Dögnitz N & Wagnières G Determination of tissue optical properties by steady-state spatial frequency-domain reflectometry. Lasers Med. Sci. 13, 55–65 (1998).

197. van de Giessen M, Angelo JP & Gioux S Real-time, profile-corrected single snapshot imaging of optical properties. Biomed. Opt. Express 6, 4051–4062 (2015). [PubMed: 26504653]

198. Vervandier J & Gioux S Single snapshot imaging of optical properties. Biomed. Opt. Express 4, 2938–2944 (2013). [PubMed: 24409392]

199. Burmeister DM et al. Utility of spatial frequency domain imaging (SFDI) and laser speckle imaging (LSI) to non-invasively diagnose burn depth in a porcine model. Burns J. Int. Soc. Burn Inj. 41, 1242–1252 (2015).

200. Greis C Technology overview: SonoVue (Bracco, Milan). Eur. Radiol 14 Suppl 8, P11–15 (2004). [PubMed: 15700328]

201. Rubaltelli L et al. Potential use of contrast-enhanced ultrasound (CEUS) in the detection of metastatic superficial lymph nodes in melanoma patients. Ultraschall Med. Stuttg. Ger. 1980 35, 67–71 (2014).

202. Swindle LD, Thomas SG, Freeman M & Delaney PM View of normal human skin in vivo as observed using fluorescent fiber-optic confocal microscopic imaging. J. Invest. Dermatol. 121, 706–712 (2003). [PubMed: 14632185]

203. Jonak C, Skvara H, Kunstfeld R, Trautinger F & Schmid JA Intradermal indocyanine green for in vivo fluorescence laser scanning microscopy of human skin: a pilot study. PLOS ONE 6, e23972 (2011). [PubMed: 21904601]

204. Piper SK et al. Towards whole-body fluorescence imaging in humans. PLOS ONE 8, e83749 (2013). [PubMed: 24391820]

205. Wapnir I et al. Intraoperative imaging of nipple perfusion patterns and ischemic complications in nipple-sparing mastectomies. Ann. Surg. Oncol. 21, 100–106 (2014). [PubMed: 24046104]

206. Cunha-Vaz J et al. Agreement between OCT leakage and fluorescein angiography to identify sites of alteration of the blood–retinal barrier in diabetes. Ophthalmol. Retina 1, 395–403 (2017). [PubMed: 31047568]

207. Najeeb BH et al. The distribution of leakage on fluorescein angiography in diabetic macular edema: a new approach to its etiology. Invest. Ophthalmol. Vis. Sci. 58, 3986–3990 (2017). [PubMed: 28796876]

208. Calvo CM & Hartnett ME The utility of ultra-widefield fluorescein angiography in pediatric retinal diseases. Int. J. Retina Vitr. 4, 21 (2018).

209. Ra H et al. In vivo imaging of human and mouse skin with a handheld dual-axis confocal fluorescence microscope. J. Invest. Dermatol. 131, 1061–1066 (2011). [PubMed: 21191407]

210. Su D et al. Seeing elastin: a near-infrared zwitterionic fluorescent probe for in vivo elastin imaging. Chem 4, 1128–1138 (2018).

211. Carr JA et al. Shortwave infrared fluorescence imaging with the clinically approved near-infrared dye indocyanine green. Proc. Natl. Acad. Sci. 115, 4465–4470 (2018). [PubMed: 29626132]

212. Wang RK Signal degradation by multiple scattering in optical coherence tomography of dense tissue: a Monte Carlo study towards optical clearing of biotissues. Phys. Med. Biol. 47, 2281–2299 (2002). [PubMed: 12164587]

213. Wang RK & Tuchin VV Optical Coherence Tomography: Light Scattering and Imaging Enhancement in Handbook of Coherent-Domain Optical Methods: Biomedical Diagnostics, Environmental Monitoring, and Materials Science (ed. Tuchin VV) 665–742 (Springer New York, 2013).

214. Zhu D, Larin KV, Luo Q & Tuchin VV Recent progress in tissue optical clearing. Laser Photonics Rev. 7, 732–757 (2013).

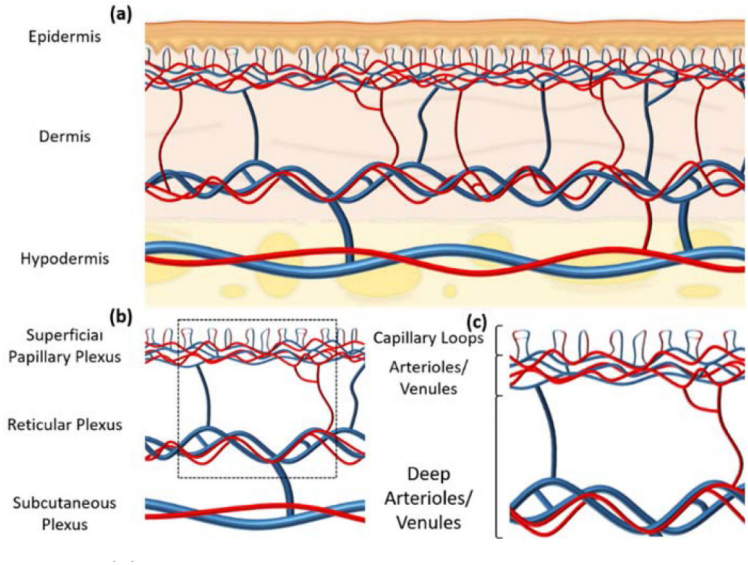

Figure 1:

Cutaneous vasculature. (a) A diagram of healthy skin highlighting three primary layers: the epidermis, the dermis, and the hypodermis. (b) A diagram highlighting the vasculature of healthy skin, again segmented into three primary layers: the superficial papillary plexus, the reticular plexus, and the subcutaneous plexus. A perforated black square highlights the vessels which are predominantly, but not exclusively, the focus of cutaneous imaging modalities. (c) A diagram highlighting the vessels of the papillary and reticular plexuses, derived from the perforated black square in (b). Shown are the capillary loops and smaller arterioles and venules of the papillary plexus, and the deeper, larger arterioles and venules of the reticular plexus.

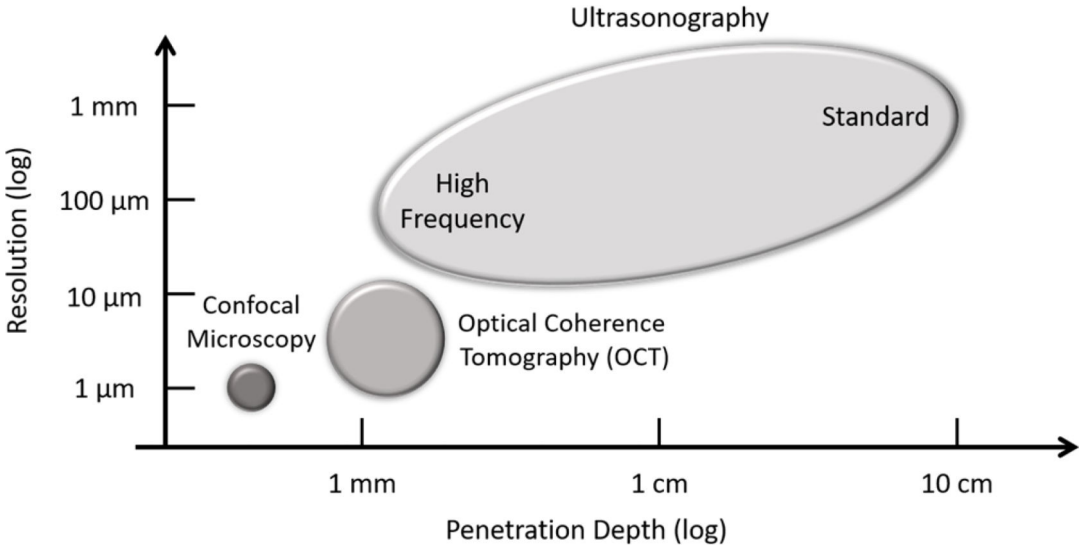

Figure 2:

A number of commonly used cutaneous imaging modalities, highlighting typical penetration depth and imaging resolution. Shown is confocal microscopy with a penetration depth of > 100 μm and resolution of 1 μm; optical coherence tomography (OCT) with a penetration depth of > 1 mm and resolution of 10 μm; and ultrasonography with a penetration depth of up to 10 cm and resolution of 10 μm. Depending upon imaging principle, a loose correlation typically exists between penetration depth and resolution; an increase in one may result in a decrease in the other.

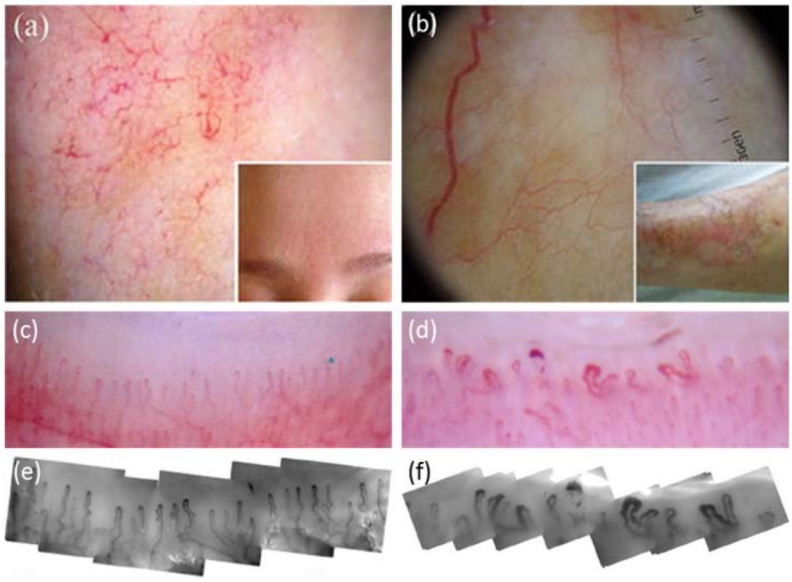

Figure 3:

Dermoscopy[46] and videocapillaroscopy[52]. (a) Dermoscopic imaging of a patient with rosacea, showing linear vessels arranged in a polygonal network. (b) Dermoscopic imaging of a patient with an advanced lesion of necrobiosis lipoidica, showing elongated, branching, and focused serpentine vessels. (c) and (d) Low magnification (10X) dermoscopic images taken of two different nailfolds. (e) and (f) High magnification (300X) videocapillaroscopic images correlating with (c) and (d), respectively. (c) and (e) were taken of a patient with primary Raynaud's phenomenon and show normal hairpin capillary loops, while (d) and (f) were taken of a patient with systemic sclerosis and show widened loops, avascularity, and haemorrhage. Permission for reuse granted for[46] under license number 4445470709458, and for[52] under the Creative Commons Attribution License.

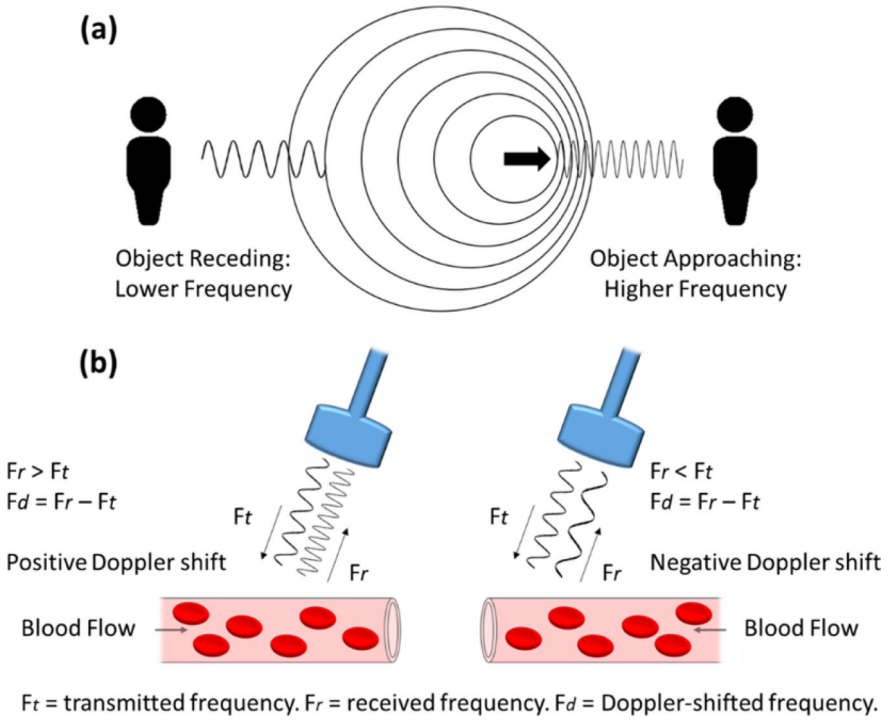

Figure 4:

The Doppler effect and how it is used to measure flow. (a) A diagram showing how the Doppler effect is perceived as a change in frequency when an object is receding from or approaching an individual. (b) A diagram showing how the Doppler effect is used to measure blood flow properties.

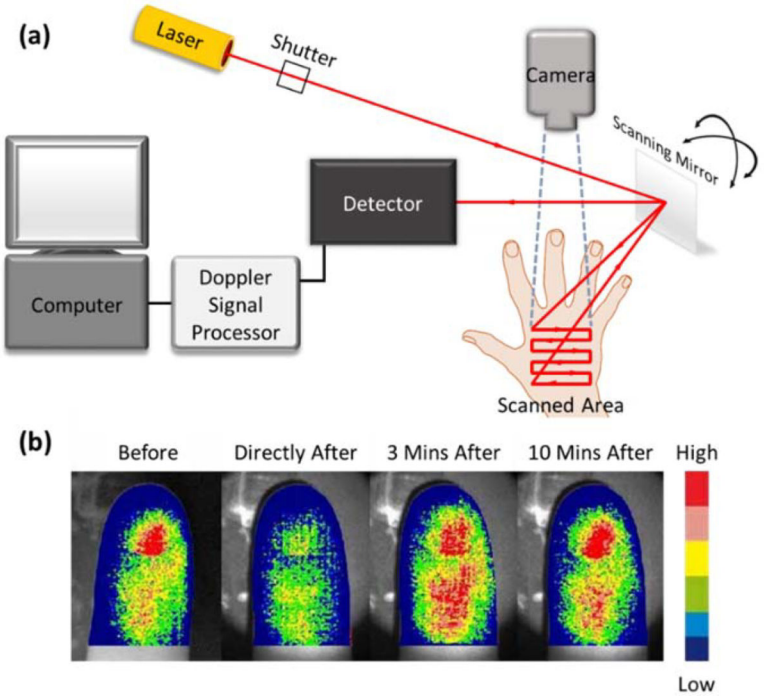

Figure 5:

Laser Doppler perfusion imaging (LDPI)[105]. (a) A schematic diagram showing the typical arrangement of an LDPI setup. (b) LDPI of an index finger before, directly after, 3 minutes after, and 10 minutes after immersion in iced-water. The 6-level color scale represents relative low – high tissue perfusion. Permission for reuse granted under the OSA Open Access Publishing Agreement.

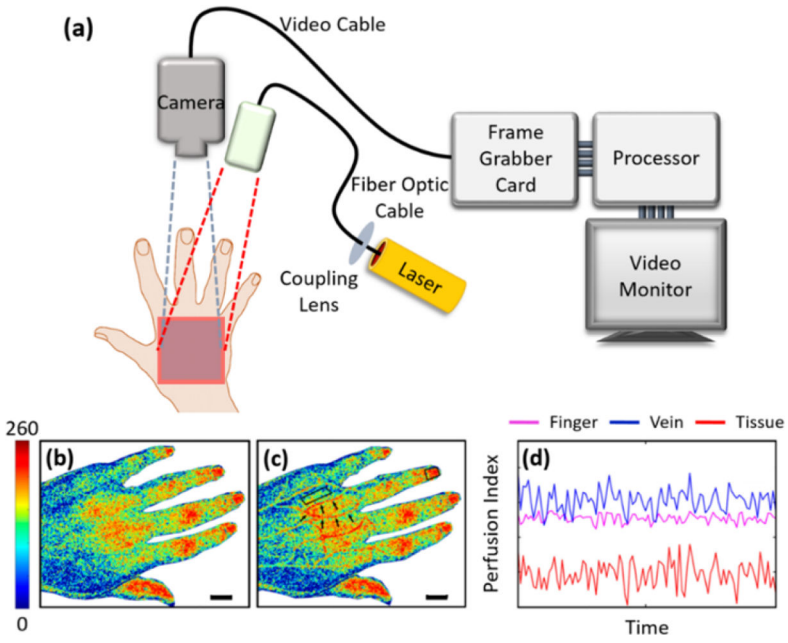

Figure 6:

Laser speckle contrast imaging (LSCI)[111]. (a) A schematic diagram showing the typical arrangement of an LSCI setup. (b) Traditional LSCI of the dorsum of a stroke patient's left hand. (c) Dual-wavelength LSCI of the same patient in (b) with regions of interest highlighted by black arrows. (d) The perfusion index signals derived from three regions of interest highlighted in (c), a finger, a vein, and skin tissue. The color scale represents the perfusion index from 0 (low) – 260 (high). Scale bar represents 15 mm. Permission for reuse granted under the Creative Commons Attribution License.

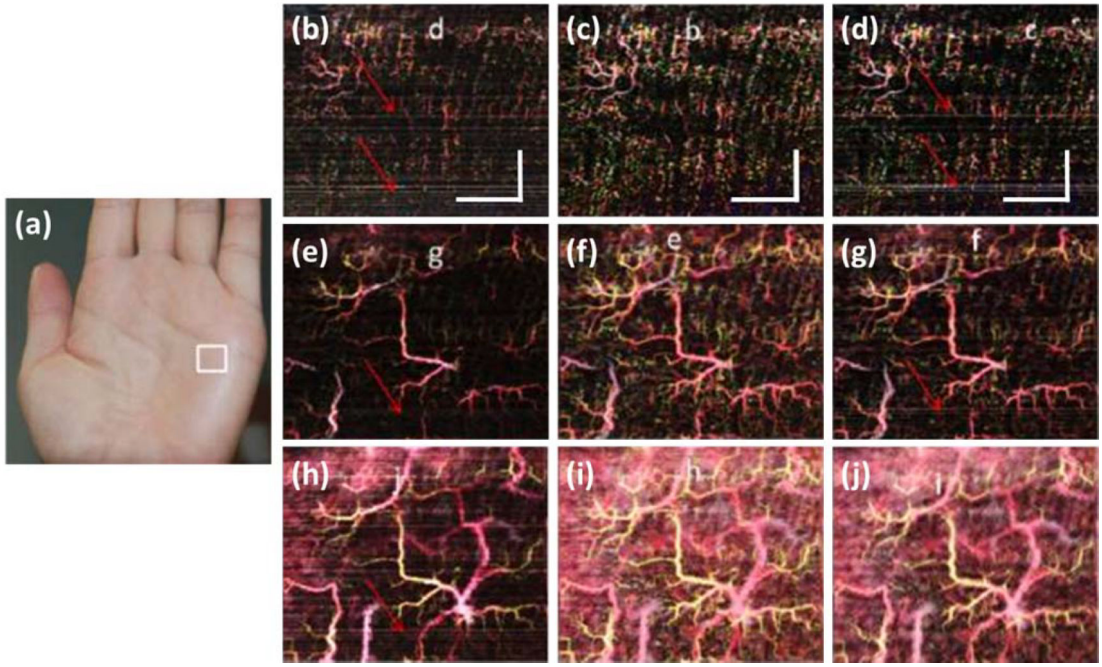

Figure 7:

Doppler optical coherence tomography (DOCT) images of the palm of an individual's hand[130]. (a) A photograph highlighting the scan area with a white box. (b) *En face* vascular image of a depth of 120 – 360 μm, derived from phase-resolved Doppler. (c) *En face* vascular image of a depth of 120 – 360 μm, derived from amplitude-resolved Doppler. (d) *En face* vascular image of a depth of 120 – 360 μm, derived from complex-resolved Doppler. (e) *En face* vascular image of a depth of 120 – 600 μm, derived from phase-resolved Doppler. (f) *En face* vascular image of a depth of 120 – 600 μm, derived from amplitude-resolved Doppler. (g) *En face* vascular image of a depth of 120 – 600 μm, derived from complex-resolved Doppler. (h) *En face* vascular image of a depth of 120 – 840 μm, derived from phase-resolved Doppler. (i) *En face* vascular image of a depth of 120 – 840 μm, derived from amplitude-resolved Doppler. (j) *En face* vascular image of a depth of 120 – 840 μm, derived from complex-resolved Doppler. Red arrows highlight bulk motion-derived artifacts that appear in the *en face* image as horizontal lines. Scale bar represents 1 mm. Permission for reuse granted under the OSA Open Access Publishing Agreement.

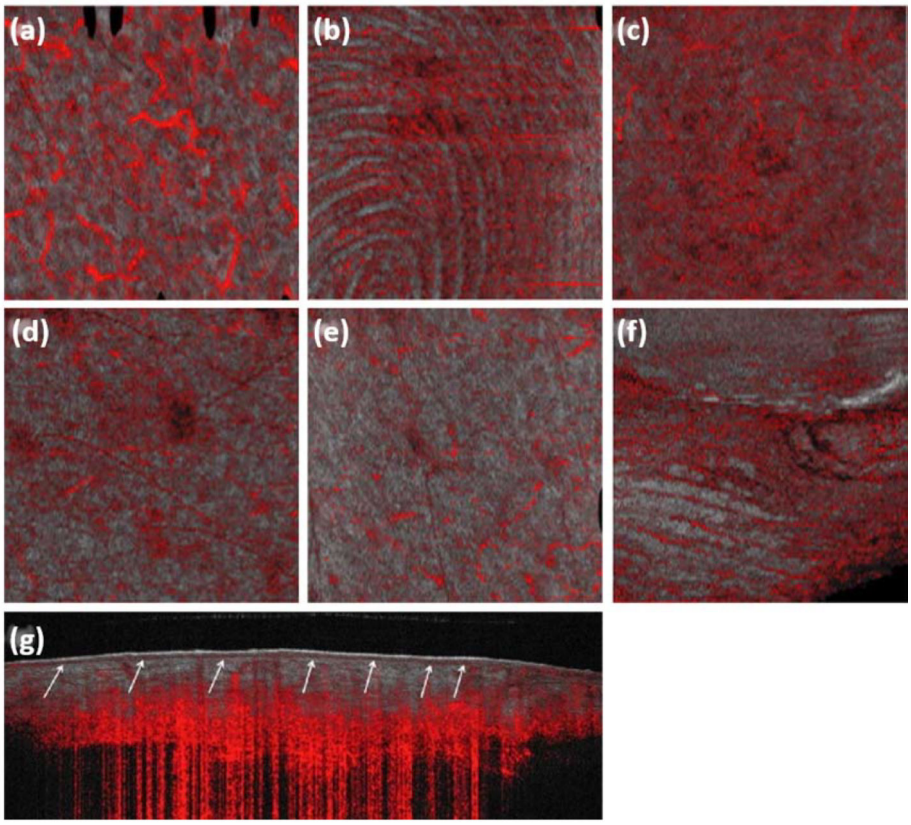

Figure 8:

Dynamic optical coherence tomography (dOCT) of the vasculature of healthy skin[11], where the *en face* OCT structural image (grey) is overlaid with vascular information (red). (a) An *en face* image of the left cheek. (b) An *en face* image of the fingertip of the left index finger. (c) An *en face* image of the right leg. (d) An *en face* image of the left arm. (e) An *en face* image of the trunk. (f) An *en face* image of the left nailfold of the left index finger. (g) A cross-sectional image of the right leg. A number of different vascular morphologies are represented, such as a live fingerprint, (b), a reticular pattern, (c), and commas and dots, (d) and (e). All *en face* images represent a field of view of 6 × 6 mm and the cross-sectional image, 6 × 2 mm. Permission for reuse granted under license number 4445471193690.

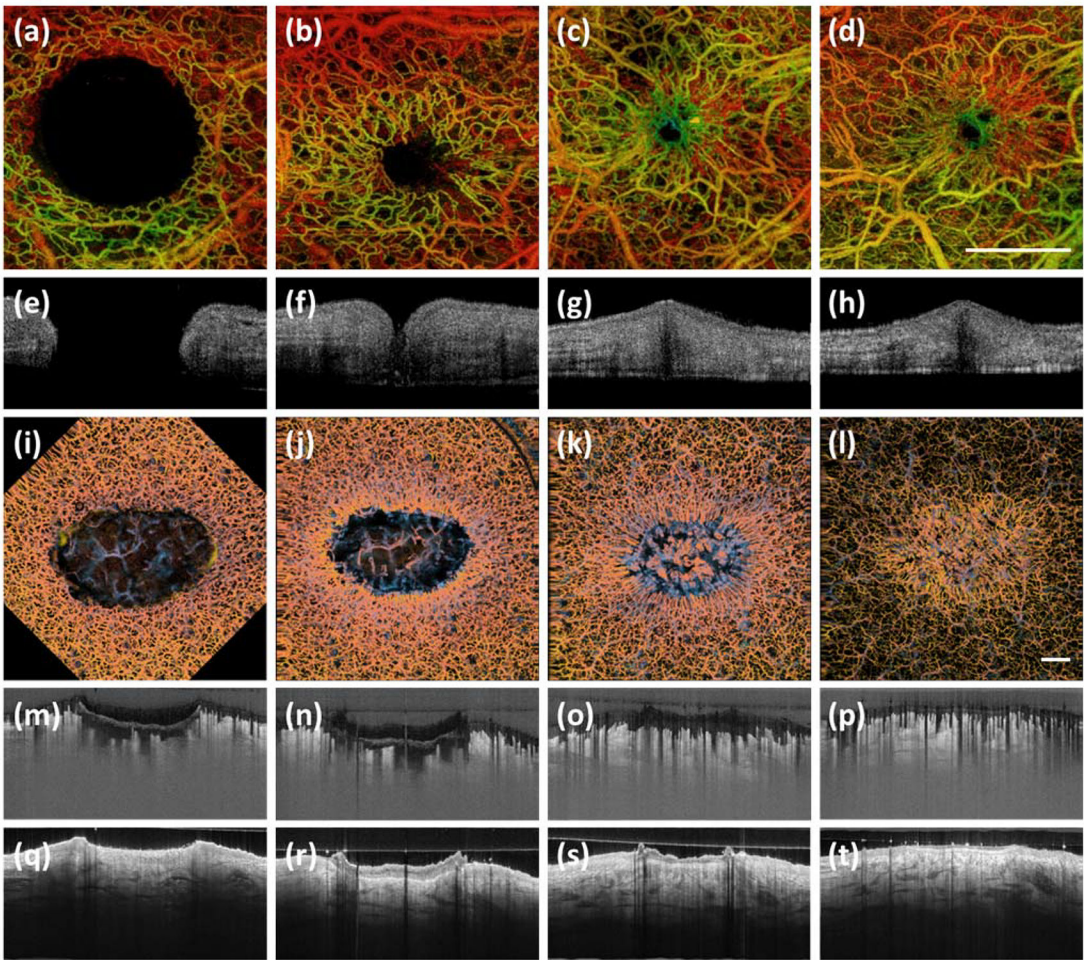

Figure 9:

Optical coherence tomography angiography (OCTA) of a murine wound model[152] and a human would model[160]. (a) – (d) Temporal *en face* OCTA images of a murine wound model healing over 7 weeks. Shown is how the microvasculature changes over the course of healing. (e) – (h) Cross-sectional images corresponding with (a) – (d), respectively. Shown are structural changes. (i) – (l) Temporal *en face* OCTA images of a human wound model healing over 6 weeks. Again, shown are the microvascular changes over the course of healing. (m) – (p) Cross-sectional images corresponding with (i) – (l), respectively. Shown are microvascular changes. (q) – (t) Cross-sectional images corresponding to (i) – (l), respectively. Shown are structural changes. Scale bar represents 1 mm. Permission for reuse granted for[152] by The International Society for Optics and Photonics (SPIE), and for[160] by the AME Publishing Company.

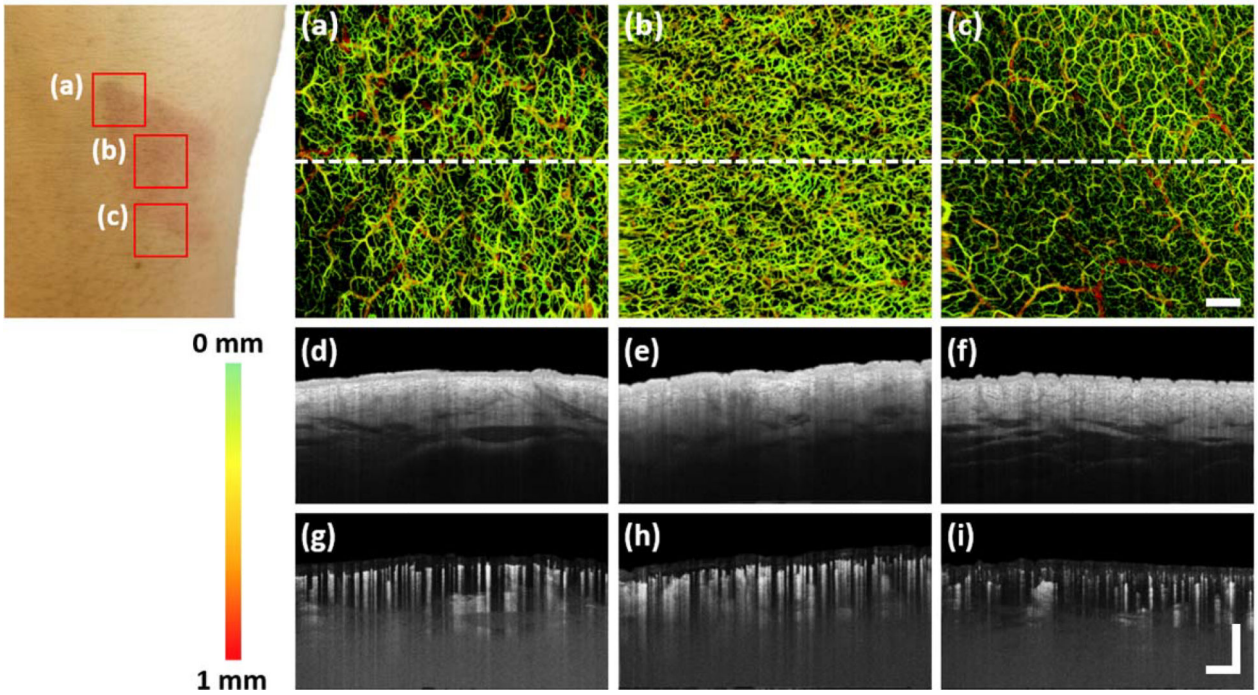

Figure 10:

Optical coherence tomography angiography (OCTA) of a scald wound 24 hours post-injury. Shown is a photograph of a scald wound on the dorsum of the right wrist. Three red boxes represent three regions of interest: (a) – (c). (a) – (c) *En face* OCTA images of the scald wound. Shown are two boundary scans, (a) and (c), and a wound center scan, (b). Clearly visible in the boundary scans are vessel density changes corresponding to the shape of the wound. Capillary density is significantly higher within the wound compared to the skin immediately surrounding the wound. (d) – (f) Cross-sectional images of the skin structure, correlating with the white perforated lines in (a) – (c), respectively. (g) – (i) Cross-sectional images of the skin's vasculature; again, correlating with the white perforated lines in (a) – (c), respectively. Vessel density here, again appears most dense within the wound. Color bar represents color-coded vessel depth. Scale bars represent 1 mm.

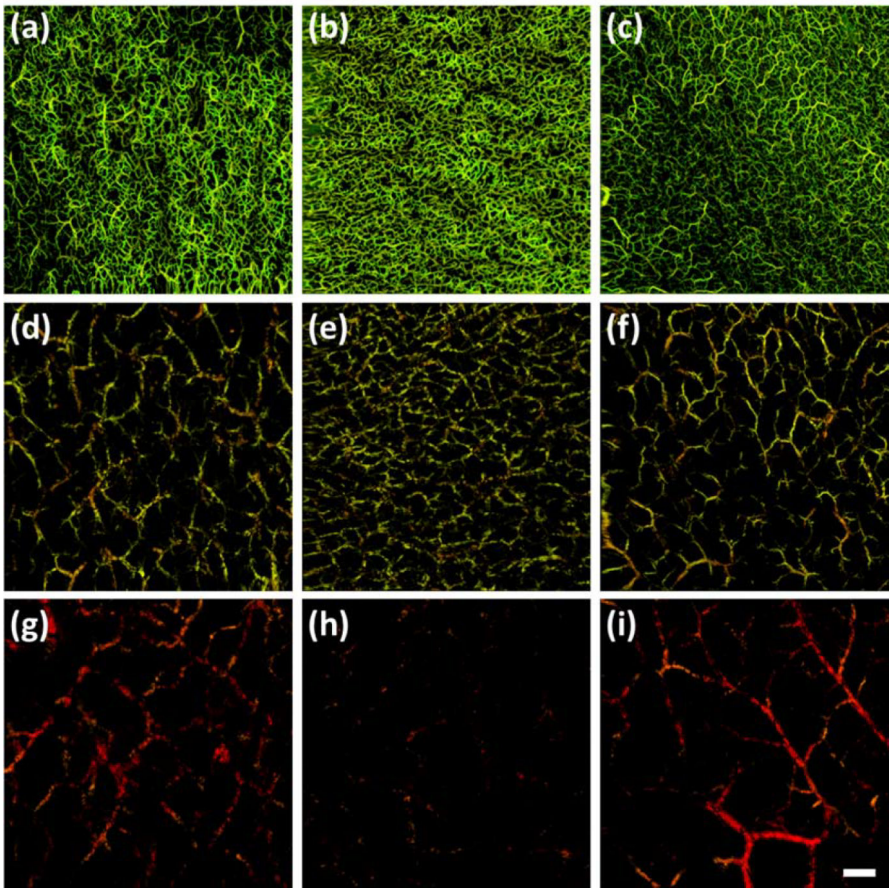

Figure 11:

Optical coherence tomography angiography (OCTA) of the same wound presented in figure 10 segmented into vascular slabs of 0 – 200 μm, 200 – 500 μm, and 500 – 1000 μm below the dermal/epidermal boundary of the skin. Such depths are thought to represent the papillary dermis, the upper reticular dermis, and the reticular dermis, respectively. (a) – (c) *En face* OCTA images of the superficial vessels of the papillary dermis (0 – 200 μm below the dermal/epidermal boundary), correlating with images (a) – (c) shown in figure 10. Visible here are vessel density changes corresponding with wound boundaries, (a) and (c), and an augmented vessel density within the wound center, (b). (d) – (f) *En face* OCTA images of the upper reticular dermis (200 – 500 μm below the dermal/epidermal boundary), correlating with (a) – (c) above, respectively. Visible again are vessel density changes between all three regions of interest. (g) – (i) *En face* OCTA images of the reticular dermis (500 – 1000 μm below the dermal/epidermal boundary), correlating with (a) – (c) above, respectively. Vascular parameters differ between all three regions of interest again. Scale bar represents 1 mm.

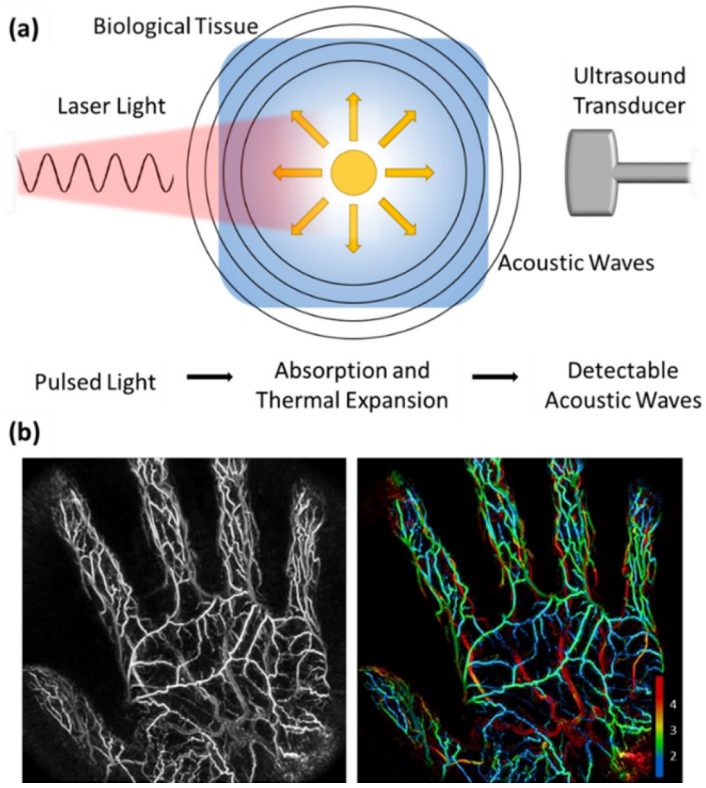

Figure 12:

A schematic of photoacoustic imaging with two example images[173]. (a) Shown is how pulsed light is absorbed by a biological tissue, which then causes thermal expansion and the emission of acoustic waves that can be detected by an ultrasound transducer. (b) A maximum intensity projected photoacoustic image of the palm of an individual's hand alongside the same image with vessel depth represented through color coding. Numbering on the bottom right of the figure represents vessel depth in mm. Permission for reuse granted under the Creative Commons Attribution License.

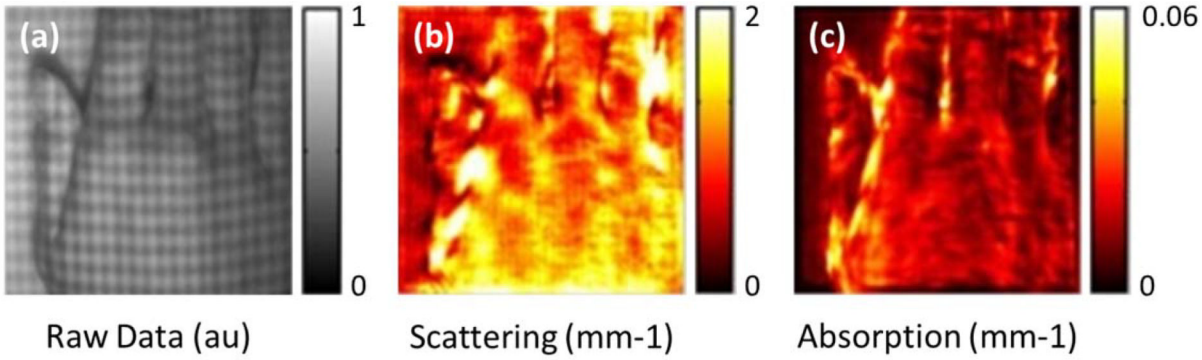

Figure 13:

SFDI imaging of an individual's right hand[197]. (a) Raw data taken by SFDI with patterned structural illumination visible. (b) A reduced scattering map derived from (a). (c) A profile-corrected absorption map derived from (a). Permission for reuse granted for[197] under the OSA Open Access Publishing Agreement.